Japan) in phosphate-buffered saline for 30 min at 37°C in a humidified chamber protected from light. Ethidium bromide was detected by fluorescent microscopy as described previously [18]. One representative section per artery was counted in all animals.

Intravascular ultrasound procedure and analysis

Twenty-three weeks after stent implantation, intravascular ultrasound imaging (IVUS) was performed. The imaging was performed using a 40 MHz ultrasonic imaging catheter (Ultra Cross; Boston Scientific, Boston, Massachusetts, USA) and an automatic pullback device, and the studies were recorded on 1/2-inch high-resolution s-VHS tapes for off-line volumetric assessment. IVUS analysis included stent area and proliferative intimal area.

Injury and inflammation scores

The injury and inflammatory scores were determined at each strut site, and mean values were calculated for each stented segment as previously described [19,20]. In brief, a numeric value from 0 (no injury) to 3 (most injury) was assigned: 0, endothelial denudate, IEL intact; 1, IEL lacerated, media compressed, not lacerated; 2, IEL lacerated, media lacerated, external elastica lamina compressed, not lacerated; and 3, media severely lacerated, external elastica lamina lacerated, adventitia may contain stent strut. The average injury score for each segment was calculated by dividing the sum of injury scores by the total number of struts at the examined section. The inflammation score took into consideration the extent and density of the inflammatory infiltrate in each individual strut. With regard to the inflammatory score for each individual strut, the grading is: 0, no inflammatory cells surrounding the strut; 1, light, non-circumferential inflammatory cells infiltrate surrounding the strut; 2, localized, moderate-to-dense cellular aggregate surrounding the strut non-circumferentially; and 3, circumferential dense inflammatory cells, infiltration of the strut. The inflammatory score for each cross section was calculated in the same manner as for the injury score (sum of the individual inflammatory scores, divided by the number of struts in the examined section).

Biochemical measurements

Biochemical parameters listed in Tables 1 and 2 were measured. MCP-1, interleukin (IL)-8, and transforming growth factor beta 1 were measured using commercially available enzyme-linked immunosorbent assay kits for humans (Quantikine R&D Systems, Minneapolis, Minnesota, USA). 8-Iso prostaglandin F2α (isoprostanes) in the urine was measured by high-performance liquid chromatography/tandem mass spectrometry as previously reported [21]. Isoprostanes were adjusted according to the creatinine level. Urine was collected over 3 h while each animal was in a metabolic cage.

Proliferation and migration assay in vascular smooth muscle cells

Human coronary artery VSMC (Cambrex Bio Science Walkersville Inc., Walkersville, Tennessee, USA) were

Table 1 Systemic biochemical parameters and body weight

		Week of experiment			
Parameters	Groups	0	8	16	24
Total cholesterol (mg/dl)	Vehicle control	430 ± 51	495 ± 51	417 ± 34	646 ± 55*
	Azel 3 mg/kg	470 ± 32	555 ± 62	524 ± 70	631 ± 42*
	Azel 10 mg/kg	437 ± 33	480 ± 47	347 ± 28	568 ± 50*
HDL-cholesterol (mg/dl)	Vehicle control	20 ± 2	19 ± 4	22 ± 6	14 ± 2
	Azel 3 mg/kg	18 ± 2	14 ± 2	15 ± 2	15 ± 2
	Azel 10 mg/kg	21 ± 4	14 ± 2	17 ± 4	16 ± 2
LDL-cholesterol (mg/dl)	Vehicle control	370 ± 46	387 ± 37	315 ± 28	512 ± 39*
	Azel 3 mg/kg	381 ± 31	430 ± 46	385 ± 46	466 ± 27*
	Azel 10 mg/kg	298 ± 32	381 ± 40	267 ± 24	420 ± 29*
Triglycerides (mg/dl)	Vehicle control	16 ± 3	16 ± 4	13 ± 1	18 ± 2
	Azel 3 mg/kg	10 ± 1	16 ± 3	13 ± 2	33 ± 9
	Azel 10 mg/kg	14 ± 1	25 ± 12	12 ± 2	25 ± 4
Glucose (mg/dl)	Vehicle control	58 ± 3	67 ± 3	64 ± 2	62 ± 3
	Azel 3 mg/kg	60 ± 4	60 ± 3	63 ± 3	66 ± 3
	Azel 10 mg/kg	65 ± 4	65 ± 3	61 ± 2	59 ± 3
GOT (unit/l)	Vehicle control	52 ± 6	44 ± 6	50 ± 4	54 ± 4
	Azel 3 mg/kg	51 ± 3	43 ± 3	47 ± 4	55 ± 3
	Azel 10 mg/kg	45 ± 4	41 ± 4	50 ± 6	61 ± 6
GPT (unit/l)	Vehicle control	29 ± 7	21 ± 3	20 ± 4	23 ± 2
	Azel 3 mg/kg	25 ± 2	20 ± 2	22 ± 7	23 ± 2
	Azel 10 mg/kg	21 ± 2	17 ± 2	17 ± 5	28 ± 6
Angiotensin II (pg/ml)	Vehicle control	29 ± 8	19 ± 4	14 ± 2	43 ± 10
	Azel 3 mg/kg	12 ± 2	15 ± 3	15 ± 3	21 ± 5
	Azel 10 mg/kg	12 ± 1	11 ± 2	15 ± 3	31 ± 8
Body weight (kg)	Vehicle control	5.2 ± 0.2	5.6 ± 0.2	6.1 ± 0.2	6.1 ± 0.2
	Azel 3 mg/kg	5.2 ± 0.2	5.6 ± 0.3	5.8 ± 0.3	5.8 ± 0.3
	Azel 10 mg/kg	5.2 ± 0.2	5.6 ± 0.2	6.0 ± 0.3	5.9 ± 0.3

Azel, azelnidipine; GOT, glutamic-oxaloacetic transaminase; GPT, glutamic-pyruvic transaminase; HDL, high-density lipoprotein; LDL, low-density lipoprotein. Data are mean ± SEM ($n = 12$ each). *$P < 0.05$ versus 0 week.

Table 2 Systemic oxidative stress marker and cytokines

Parameters	Groups	Week of experiment			
		0	8	16	24
8-Iso-prostaglandin in urine (ng/mg creatinine)	No treatment	716 ± 86	691 ± 94	654 ± 75	603 ± 88
	Azel 3 mg/kg	714 ± 78	572 ± 92	621 ± 86	626 ± 66
	Azel 10 mg/kg	845 ± 79	674 ± 98	693 ± 92	573 ± 78*
MCP-1 in serum (pg/ml)	No treatment	44 ± 5	40 ± 11	51 ± 3	61 ± 5*
	Azel 3 mg/kg	46 ± 3	37 ± 8	45 ± 3	47 ± 5
	Azel 10 mg/kg	47 ± 4	32 ± 7	29 ± 5†*	37 ± 4†*
IL-8 in serum (ng/ml)	No treatment	3.0 ± 0.3	3.8 ± 0.5	4.4 ± 0.5	3.2 ± 0.5
	Azel 3 mg/kg	2.2 ± 0.3	2.9 ± 0.3	4.6 ± 0.4	3.6 ± 0.7
	Azel 10 mg/kg	2.7 ± 0.3	3.3 ± 0.4	4.2 ± 0.8	2.7 ± 0.6
TGF-β1 in serum (ng/ml)	No treatment	63 ± 6	70 ± 7	67 ± 7	47 ± 4
	Azel 3 mg/kg	55 ± 4	67 ± 3	68 ± 7	43 ± 5
	Azel 10 mg/kg	56 ± 4	73 ± 4	62 ± 4	42 ± 3

Azel, azelnidipine; IL, interleukin; MCP-1, Monocyte chemoattractant protein 1; TGF-β1, transforming growth factor beta 1. Data are mean ± SEM ($n = 12$ each). *$P < 0.01$ versus 0 week, †$P < 0.05$ versus no treatment group.

cultured, and placed into 48-well culture plates (Falcon 354506 Biocoat Cell Ware Human Fibronectin; Bioscience Inc., Bedford Massachusetts, USA). Proliferation was stimulated by human MCP-1 at 10 ng/ml (Sigma). Azelnidipine at 1, 10, and 100 nmol or solvent were added to the wells. Four days later, the cells were fixed with methanol and a single observer, who was blinded to the experimental protocol, counted the number of cells per plate.

The migration of rat aortic smooth muscle cells was assessed with a Boyden chamber type cell migration assay kit housing a collagen-precoated polycarbonate membrane with 8.0-μm pores (Chemicon International Inc., Termacula, California, USA), as previously described [22]. The lower chambers were filled with or without human MCP-1 at 10 ng/ml (Sigma). Then cells (1×10^5 cells/ml) were placed on the upper side of the membrane and allowed to migrate through the pores. After 4 h of incubation, the number of cells that migrated to the lower surface of the membrane was counted per ×200 high-power fields. Azelnidipine at 1, 10, and 100 nmol or solvent was added to the lower chamber.

The concentrations of azelnidipine at ranges of 1–10 nmol can be considered as a clinically relevant dose, because the concentrations are nearly equivalent to the concentration reported in human subjects who were orally administered a 5 or 15 mg azelnidipine tablet [23].

Measurements of arterial blood pressure, heart rate, and plasma azelnidipine levels

Separate preliminary experiments were performed to determine the effects of azelnidipine on arterial blood pressure and heart rate in cynomolgus monkeys under conscious conditions. On the last day of the drug treatment period, blood samples were drawn before and after drug administration, and the plasma drug concentration was determined by gas chromatography–mass spectrometry [15].

Statistical analysis

Data are expressed as the mean ± SE. Statistical analysis of differences was compared by analysis of variance and Dunnet's multiple comparison tests. A P value of less than 0.05 was considered to be statistically significant.

Results

General status

No animals showed any adverse clinical signs (decreased spontaneous motor action, decreased food consumption, diarrhoea, limping and prone position, etc.) during the experimental period and all survived. There was no significant treatment effect on body weight among the groups (Table 1).

Histopathological and immunohistochemical analysis, and detection of local oxidative stress

There were no significant differences in stent area, IEL length, and medial area among all three groups (Fig. 2). Azelnidipine at the high dose tended to decrease the neointimal area (vehicle group, 2.4 ± 0.2; low-dose group, 2.3 ± 0.2; high-dose group, 1.8 ± 0.2 mm^2; vehicle versus high dose $P = 0.07$) and significantly decreased neointimal thickening (vehicle group, 0.25 ± 0.02; low-dose group, 0.24 ± 0.02; high-dose group, 0.19 ± 0.02; vehicle versus high dose $P < 0.05$; Fig. 2).

Both MCP-1 and CCR2 immunoreactivity was not detected in the non-stented normal artery (data not shown). In contrast, intense MCP-1 and CCR2 immunoreactivity was evident in the neointima and media of stented arteries from the control group. The percentage of MCP-1-positive cells in the neointima decreased in the high-dose azelnidipine group (Fig. 3), whereas the percentage of CCR2-positive cells did not differ among the three groups. In contrast, there was no significant difference in the percentage of MCP-1 or CCR2-positive cells in the media among the three groups.

Local oxidative stress was measured with dihydroethidium staining. No apparent dihydroethidium fluorescence

Fig. 2

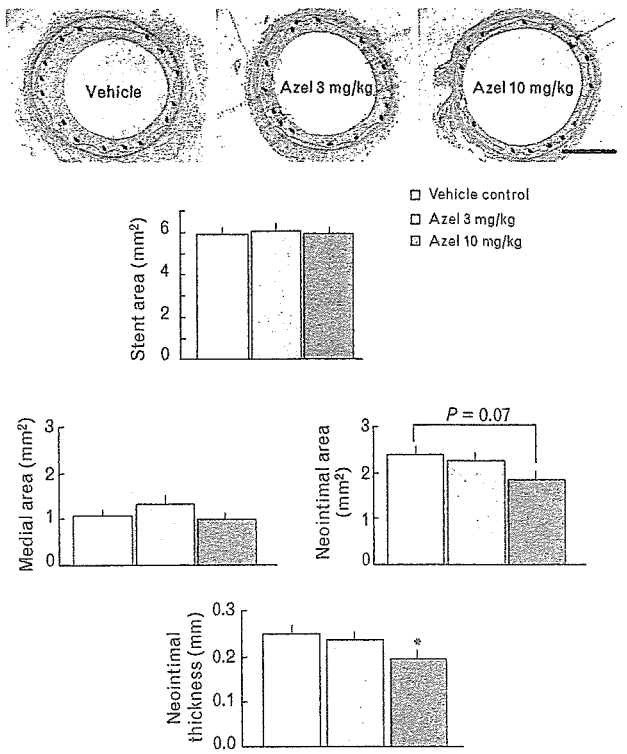

Effects of azelnidipine on stent-associated neointimal formation (histopathological analysis). (a) Representative photomicrographs of cross-sections of the stented iliac artery stained with elastica van Gieson from vehicle control group (left panel), low-dose azelnidipine (Azel) group (middle panel), and high-dose azelnidipine group (right panel) 24 weeks after stenting. Bar 1 mm. (b) Stent area (area within the stent itself), medial area (area within the external elastica lamina minus internal elastica lamina area), neointimal area (area within the internal elastica lamina minus lumen area), and neointimal thickening ($n = 12$ each). $^*P < 0.05$ versus vehicle group. Each value represents mean ± SEM.

Fig. 3

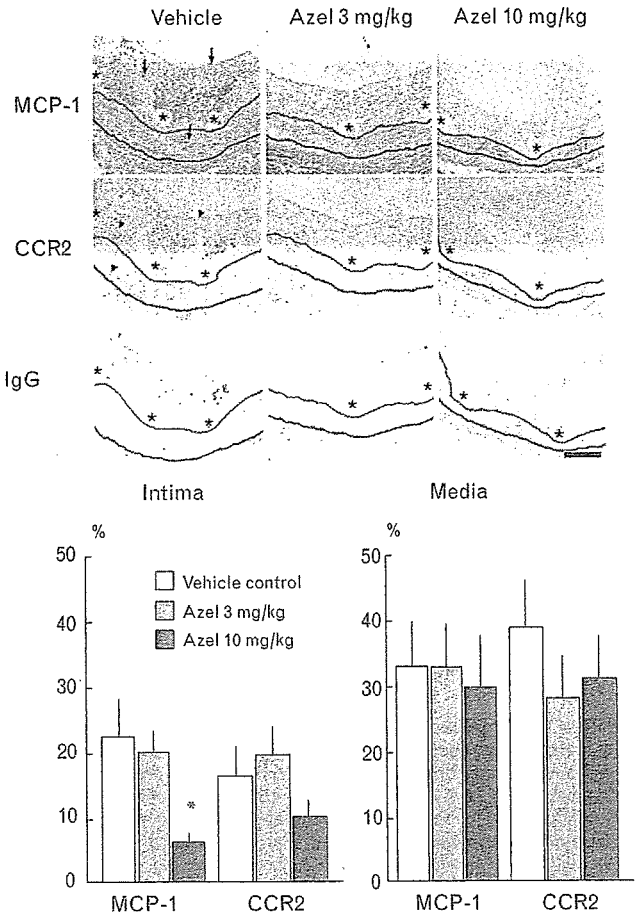

Effects of azelnidipine (Azel) on immunoreactivity for monocyte chemoattractant protein 1 (MCP-1) and C-C chemokine receptor 2 (CCR2). (a) Cross-sections of stented arteries from experimental groups stained immunohistochemically with the antibody against MCP-1 (arrows), CCR2 (arrow heads) or non-immune IgG (* indicates stent strut sites). White and blue lines show internal and external elastica lamina, respectively. (b) The percentages of MCP-1 and CCR2-positive cells in the neointima and media ($n = 12$ each). Bar 100 μm. $^*P < 0.05$ versus vehicle group. Each value represents mean ± SEM.

was detected in the non-stented normal artery (data not shown). As shown in Fig. 4, the fluorescent signal attributable to superoxide production was markedly enhanced in the neointima and media from the control group. The intensity of dihydroethidium fluorescence in the neointima decreased in the high-dose azelnidipine group, whereas the dihydroethidium signal in the media did not differ among the three groups (Fig. 4).

Injury score, inflammation score, and neovascularization

There was no significant difference in the injury score and inflammation score between the three groups (Fig. 5). Also, there were no significant differences in the degrees of neovascularization in the neointima (vWF-positive microvessels/mm^2) and adventitia (vWF-positive microvessels/section; Fig. 5).

Intravascular ultrasound imaging analysis

The degrees of neointimal formation were also investigated by IVUS analysis. As shown in histopathological analysis, high-dose azelnidipine reduced stent-associated neointimal formation by 42% (Fig. 6).

Systemic biochemical parameters

Low and high doses of azelnidipine also did not affect lipid profiles, angiotensin II and liver transaminases (Table 1). Azelnidipine at the high dose decreased 8-iso-prostaglandin F2α in urine at week 24 (Table 2). Serum levels of MCP-1 increased at week 24 in the vehicle group (Table 2). No increase in serum MCP-1 levels was noted in azelnidipine treatment groups. Notably, azelnidipine at the high dose reduced serum MCP-1 levels. In contrast, there were no treatment effects of azelnidipine on serum levels of IL-8 and transforming growth factor beta 1 (Table 2).

Fig. 4

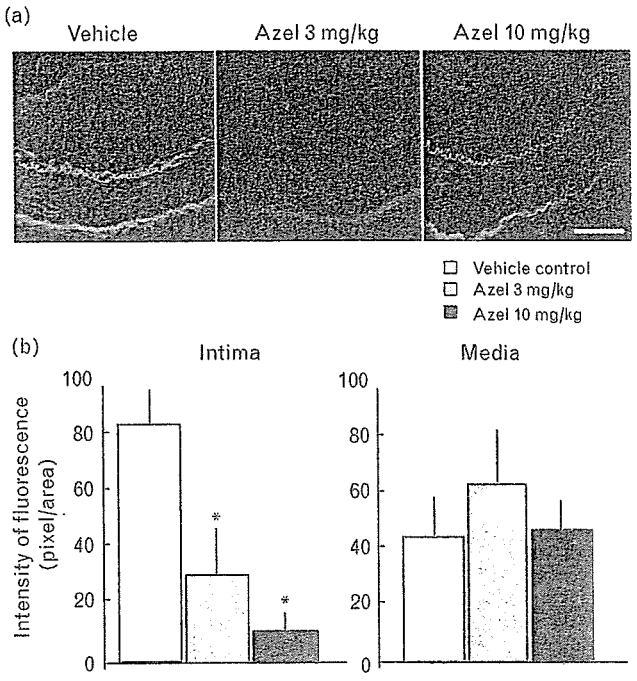

Effects of azelnidipine (Azel) on local oxidative stress marker. (a) Representative superoxide detection with dihydroethidium in cross-sections of iliac arteries. Red colour expressed dihydroethidium-stained positive nuclei, and yellow or green expressed autofluorescences. Autofluorescences were agreed internal elastica lamina (upper line) and external elastica lamina (lower line). Bar 100 μm. (b) Mean fluorescent intensity in the neointima and media ($n = 12$ each). *$P < 0.01$ versus vehicle group. Each value represents mean ± SEM.

Fig. 5

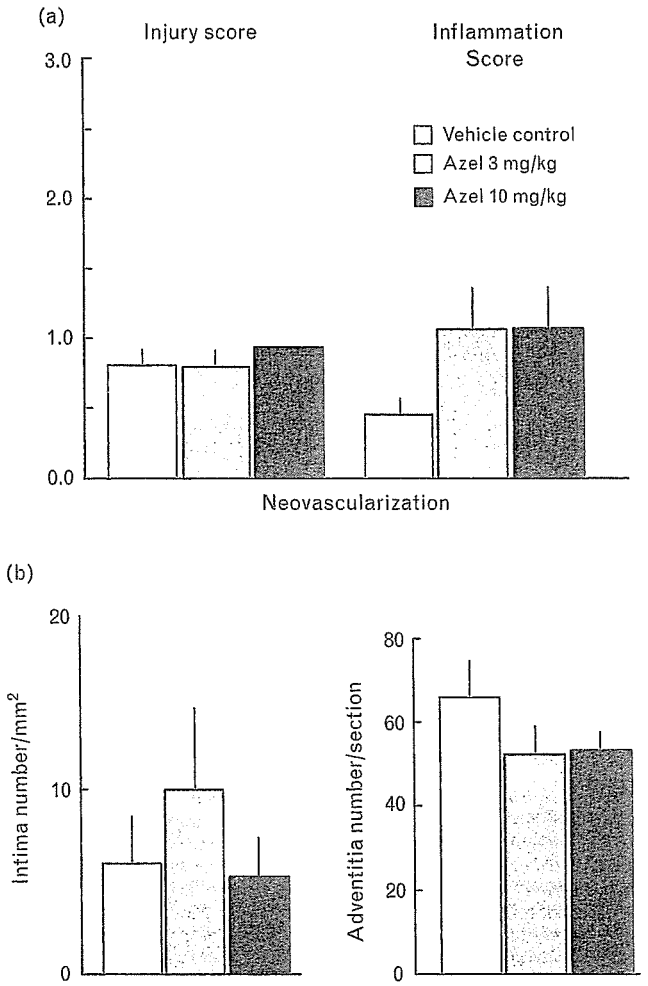

Effects of azelnidipine (Azel) on injury score, inflammation score, and neovascularization. (a) Injury score and inflammation score. (b) The degrees of neovascularization in the neointima and adventitia. The neovascularization were defined as von Willebrand factor (vWF)-positive microvessels/mm^2 in the neointima and vWF-positive microvessels/section in adventitia ($n = 12$ each). Each value represents mean ± SEM.

Proliferation and migration assay of vascular smooth muscle cells

Azelnidipine at 1, 10, and 100 nmol significantly inhibited MCP-1-induced proliferation in a dose-dependent manner (Fig. 7). Azelnidipine also reduced the MCP-1-induced migration of rat aortic smooth muscle cells (Fig. 7).

Haemodynamic parameters and plasma azelnidipine concentrations

Azelnidipine at the low and high doses did not affect haemodynamic parameters (Table 3). The maximum concentration (C_{max}) of azelnidipine at 3 and 10 mg/kg per day was 36 ± 17 and 107 ± 17 ng/ml, respectively, in monkeys. The C_{max} after oral administration of azelnidipine at 16 mg in hypertensive individuals is reported to be 48 ± 19 ng/ml [15].

Discussion

The present study demonstrated for the first time that a newly developed calcium antagonist, azelnidipine, at 10 mg/kg attenuated neointimal formation 6 months after stent implantation in hypercholesterolemic non-human primates (cynomolgus monkeys). We evaluated the degrees of stent-associated neointimal formation in two ways: histopathological and IVUS analyses. Both methods demonstrated significant benefits of azelnidipine by reducing neointimal formation after stent implantation. Although an appropriate animal model for the evaluation of stent-associated neointimal formation (restenotic changes) is uncertain, the non-human primate model may gain the advantage over non-primate animal models such as rabbits and pigs, because adequate degrees of neointima develop after stenting, and vascular inflammatory and proliferative responses to injury in non-human primates are presumed to be closer to those in humans than other non-primate models. Therefore, the use of non-human primates may allow us to evaluate the efficacy of any therapies on

Fig. 6

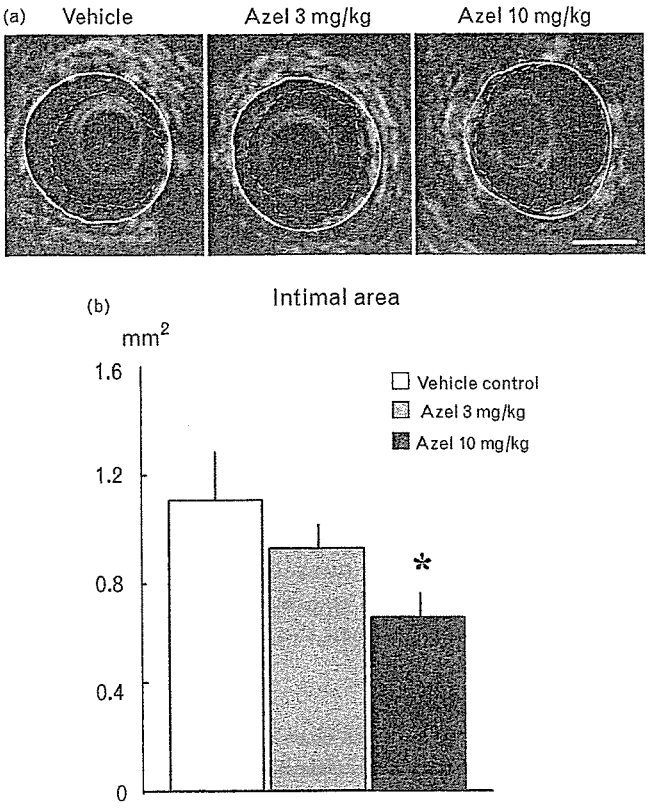

Effects of azelnidipine (Azel) on stent-associated neointimal formation by intravascular ultrasound analysis. (a) An intravascular ultrasound cross-sectional image in the treatment groups. Dot lines and solid lines show endothelial and internal elastica lamina, respectively. Bar 1 mm. (b) Effect of azelnidipine on neointimal area ($n = 8-10$ each). $^{*}P < 0.05$ versus vehicle group. Each value represents mean ± SEM.

Fig. 7

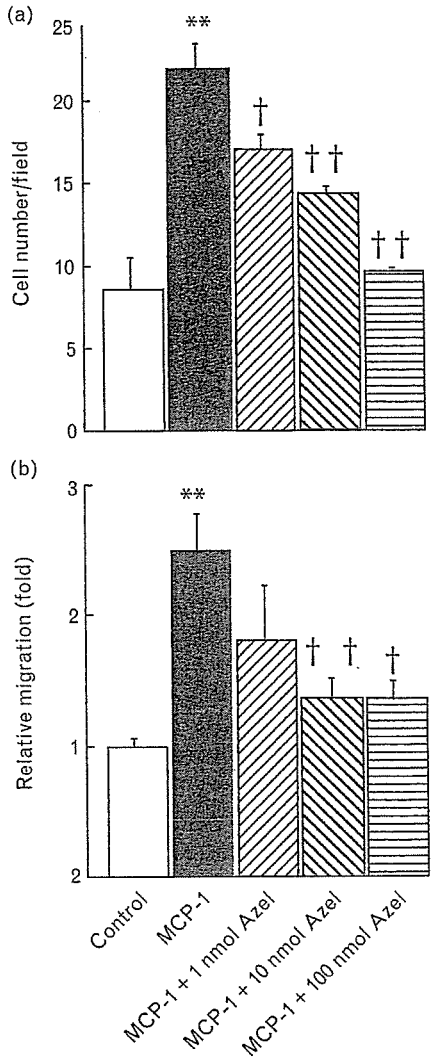

Effects of azelnidipine (Azel) on proliferation of human coronary artery smooth muscle cells (a) and on the migration of rat aortic smooth muscle cells (b). $^{*}P < 0.05$, $^{**}P < 0.01$ versus control. $^{\dagger}P < 0.05$, $^{\dagger\dagger}P < 0.01$ versus monocyte chemoattractant protein 1 (MCP-1; $n = 9$ each). Each value represents mean ± SEM.

stent-associated neointimal formation in clinically relevant conditions.

Another important point is that the both doses of azelnidipine did not significantly reduce arterial blood pressure in cynomolgus monkeys (Table 3). Furthermore, azelnidipine did not affect serum lipid levels (Table 1). Therefore, the beneficial effect of azelnidipine on stent-associated neointimal formation was independent of its effects on serum lipid or arterial blood pressure. Although the reason why the high dose of azelnidipine, which was higher than the clinical dose in respect of plasma concentrations (C_{max}), did not reduce arterial blood pressure, it might be explained by a species difference. In addition, the fact

Table 3 Mean heart rate and blood pressure in conscious cynomolgus monkeys treated with or without azelnidipine

	Vehicle control	Azelnidipine 3 mg/kg per day	Azelnidipine 10 mg/kg per day
Heart rate (beats/min)	123 ± 11	146 ± 12	147 ± 10
Systolic blood pressure (mmHg)	101 ± 5	100 ± 4	98 ± 3
Diastolic blood pressure (mmHg)	70 ± 3	68 ± 2	64 ± 2

Data are expressed as mean ± SEM. Cynomolgus monkeys (three males and three females) were sedated with intramuscular ketamine. A telemetry transmitter system with a catheter-type pressure manometer (TL11M2-D70-PCT; Data Sciences International, Arden Hills, Minnesota, USA) was implanted at the subcutaneous space of the abdomen, and the tip of the manometer was placed in the abdominal aorta through the femoral artery. After the animals recovered from the surgery and stabilized, arterial blood pressure and heart rate were continuously measured for at least 48 h by a telemetry receiver system (Data Sciences International) before and 7 days after the oral administration of azelnidipine at 3 or 10 mg/kg per day. Mean systolic blood pressure, diastolic blood pressure, and heart rate were examined with a computer-based analysis system equipped with a telemetry system (Primetech Inc., Tokyo, Japan).

that normotensive monkeys were used in the present study can be explored.

To investigate the potential mechanisms of the beneficial action of azelnidipine, we examined the systemic and local oxidative stress markers. Azelnidipine at 10 mg/kg slightly but significantly reduced the systemic marker (urine isoprostanes) 24 weeks after stent implantation. However, the effect of azelnidipine on systemic oxidative stress is not conclusive because of the variability of baseline values. In contrast, a representative local marker (fluorescent dihydroethidium staining) was reduced in neointimal cells (VSMC), but not in medial cells by azelnidipine at 10 mg/kg. These data support the notion that local oxidative stress in activated neointimal smooth muscle cells is important as one of the major mechanisms underlying the vasculoprotective action of azelnidipine seen in the present study.

It is now known that the oxidative stress-induced inflammatory and proliferative process is a centre stage of neointimal formation after vascular injury [24,25]. We and others have demonstrated that increased monocyte-mediated inflammation is associated with greater neointimal formation after stenting [26,27], and anti-MCP-1 gene therapy [12,14,28,29] or the administration of blocking antibody against the MCP-1 receptor [30] markedly reduced neointimal formation after vascular injury. In the present study, we therefore examined MCP-1 expression and showed a reduction in serum MCP-1 levels and MCP-1 immunoreactivity in the neointima by azelnidipine at 10 mg/kg. These data suggest that the vasculoprotective effects of azelnidipine may be attributable to the inhibition of the oxidative stress-induced upregulation of MCP-1. However, because there were no significant differences in the inflammation score, injury score, and neovascularization between the three groups, it is suggested that the beneficial effects of azelnidipine cannot be explained solely by its anti-inflammatory actions.

Emerging evidence, however, suggests that MCP-1 not only mediates monocyte-related inflammation, but also mediates the transformation, proliferation, and migration of VSMC [31–33]. We therefore hypothesized that azelnidipine inhibits the proliferation/migration of VSMC induced by MCP-1. Our present data with VSMC in culture suggest that azelnidipine might attenuate stent-associated neointimal formation at least partly by inhibiting the proliferation and migration of VSMC induced by MCP-1.

Our present data suggest that azelnidipine attenuated the proliferation and migration of VSMC in the neointima and thus decreased the production of inflammatory cytokines and growth factors after stent intervention, which in turn led to reduced neointimal formation. It has been suggested that azelnidipine might be used for the prevention or treatment of atherosclerotic vascular disease after stenting procedures as a 'vasculoprotective calcium antagonist'. A drug-eluting stent is now becoming a major therapeutic device for patients with flow-limiting vascular stenosis. It is expected that oral azelnidipine treatment in addition to a drug-eluting stent would further decrease restenosis and clinical outcomes in patients.

In conclusion, this study provided experimental evidence suggesting that oral treatment with azelnidipine attenuates stent-associated neointimal formation in non-human primates. The beneficial effects were associated with reduced local oxidative stress, MCP-1 expression and smooth muscle cell proliferation/migration in the neointima. These data in non-human primates suggest the potential clinical benefits of azelnidipine as a 'vasculoprotective calcium antagonist' in patients undergoing vascular interventions. However, further clinical research is needed to support this notion, because the effective dose of azelnidipine was higher than the clinical dose range.

Acknowledgments

The authors would like to thank M. Jichu, M.Yamamoto, E. Iwata, J. Luo and E. Suzuki for excellent technical assistance.

References

1 Pitt B, Byington RP, Furberg CD, Hunninghake DB, Mancini GB, Miller ME, Riley W. Effect of amlodipine on the progression of atherosclerosis and the occurrence of clinical events. PREVENT Investigators. *Circulation* 2000; **102**:1503–1510.

2 The ALLHAT Officers and Coordinators for the ALLHAT Collaborative Research Group. Major outcomes in high-risk hypertensive patients randomized to angiotensin-converting enzyme inhibitor or calcium channel blocker vs diuretic: the Antihypertensive and Lipid-Lowering Treatment to Prevent Heart Attack Trial (ALLHAT). *JAMA* 2002; **288**:2981–2997.

3 Julius S, Kjeldsen SE, Weber M, Brunner HR, Ekman S, Hansson L, *et al.* Outcomes in hypertensive patients at high cardiovascular risk treated with regimens based on valsartan or amlodipine: the VALUE randomised trial. *Lancet* 2004; **363**:2022–2031.

4 Jorgensen B, Simonsen S, Endresen K, Forfang K, Vatne K, Hansen J, *et al.* Restenosis and clinical outcome in patients treated with amlodipine after angioplasty: results from the Coronary AngioPlasty Amlodipine REStenosis Study (CAPARES). *J Am Coll Cardiol* 2000; **35**:592–599.

5 Nissen SE, Tuzcu EM, Libby P, Thompson PD, Ghali M, Garza D, *et al.* Effect of antihypertensive agents on cardiovascular events in patients with coronary disease and normal blood pressure: the CAMELOT study: a randomized controlled trial. *JAMA* 2004; **292**:2217–2225.

6 Mason RP, Marche P, Hintze TH. Novel vascular biology of third-generation L-type calcium channel antagonists: ancillary actions of amlodipine. *Arterioscler Thromb Vasc Biol* 2003; **23**:2155–2163.

7 Cristofori P, Lanzoni A, Quartaroli M, Pastorino AM, Zancanaro C, Cominacini L, *et al.* The calcium-channel blocker lacidipine reduces the development of atherosclerotic lesions in the apoE-deficient mouse. *J Hypertens* 2000; **18**:1429–1436.

8 Suzuki J, Iwai M, Li Z, Li JM, Min LJ, Ide A, *et al.* Effect of combination of calcium antagonist, azelnidipine, and AT1 receptor blocker, olmesartan, on atherosclerosis in apolipoprotein E-deficient mice. *J Hypertens* 2005; **23**:1383–1389.

9 Kataoka C, Egashira K, Ishibashi M, Inoue S, Ni W, Hiasa KI, *et al.* Novel anti-inflammatory actions of amlodipine in a rat model of arteriosclerosis induced by long-term inhibition of nitric oxide synthesis. *Am J Physiol Heart Circ Physiol* 2004; **286**:H768–H774.

10 Kim-Mitsuyama S, Izumi Y, Izumiya Y, Yoshida K, Yoshiyama M, Iwao H. Additive beneficial effects of the combination of a calcium channel blocker and an angiotensin blocker on a hypertensive rat-heart failure model. *Hypertens Res* 2004; **27**:771–779.
11 Ide S, Kondoh M, Satoh H, Karasawa A. Anti-proliferative effects of benidipine hydrochloride in porcine cultured vascular smooth muscle cells and in rats subjected to balloon catheter-induced endothelial denudation. *Biol Pharm Bull* 1994; **17**:627–631.
12 Ohtani K, Usui M, Nakano K, Kohjimoto Y, Kitajima S, Hirouchi Y, *et al.* Antimonocyte chemoattractant protein-1 gene therapy reduces experimental in-stent restenosis in hypercholesterolemic rabbits and monkeys. *Gene Ther* 2004; **11**:1273–1282.
13 Costa MA, Simon DI. Molecular basis of restenosis and drug-eluting stents. *Circulation* 2005; **111**:2257–2273.
14 Egashira K. Molecular mechanisms mediating inflammation in vascular disease: special reference to monocyte chemoattractant protein-1. *Hypertension* 2003; **41**:834–841.
15 Kuramoto K, Ichikawa S, Hirai A, Kanada S, Nakachi T, Ogihara T. Azelnidipine and amlodipine: a comparison of their pharmacokinetics and effects on ambulatory blood pressure. *Hypertens Res* 2003; **26**: 201–208.
16 Koike H, Kimura T, Kawasaki T, Sada T, Ikeda T, Sanbuissho A, Saito H. Azelnidipine, a long-acting calcium channel blocker with slow onset and high vascular affinity. *Annu Rep Sankyo Res Lab* 2002; **54**:1–64.
17 Yagil Y, Lusting A. Azelnidipine (CS-905), a novel dihydropyridine calcium channel blocker with gradual onset and prolonged duration of action. *Cardiovasc Drugs Rev* 1995; **13**:137–148.
18 Iwai M, Liu HW, Chen R, Ide A, Okamoto S, Hata R, *et al.* Possible inhibition of focal cerebral ischemia by angiotensin II type 2 receptor stimulation. *Circulation* 2004; **110**:843–848.
19 Schwartz RS, Huber KC, Murphy JG, Edwards WD, Camrud AR, Vlietstra RE, Holmes DR. Restenosis and the proportional neointimal response to coronary artery injury: results in a porcine model. *J Am Coll Cardiol* 1992; **19**:267–274.
20 Kornowski R, Hong MK, Tio FO, Bramwell O, Wu H, Leon MB. In-stent restenosis: contributions of inflammatory responses and arterial injury to neointimal hyperplasia. *J Am Coll Cardiol* 1998; **31**:224–230.
21 Ohashi N, Yoshikawa M. Rapid and sensitive quantification of 8-isoprostaglandin F2alpha in human plasma and urine by liquid chromatography-electrospray ionization mass spectrometry. *J Chromatogr B Biomed Sci Appl* 2000; **746**:17–24.
22 Ono H, Ichiki T, Fukuyama K, Iino N, Masuda S, Egashira K, Takeshita A. cAMP-response element-binding protein mediates tumor necrosis factor-alpha-induced vascular smooth muscle cell migration. *Arterioscler Thromb Vasc Biol* 2004; **24**:1634–1639.
23 Azelnidipine. CS 905, Calblock, RS 9054. *Drugs R D* 2003; **4**:122–125.
24 Egashira K. Clinical importance of endothelial function in arteriosclerosis and ischemic heart disease. *Circ J* 2002; **66**:529–533.
25 Griendling KK, FitzGerald GA. Oxidative stress and cardiovascular injury. Part II: animal and human studies. *Circulation* 2003; **108**: 2034–2040.
26 Farb A, Weber DK, Kolodgie FD, Burke AP, Virmani R. Morphological predictors of restenosis after coronary stenting in humans. *Circulation* 2002; **105**:2974–2980.
27 Welt FG, Rogers C. Inflammation and restenosis in the stent era. *Arterioscler Thromb Vasc Biol* 2002; **22**:1769–1776.
28 Usui M, Egashira K, Ohtani K, Kataoka C, Ishibashi M, Hiasa K, *et al.* Anti-monocyte chemoattractant protein-1 gene therapy inhibits restenotic changes (neointimal hyperplasia) after balloon injury in rats and monkeys. *FASEB J* 2002; **16**:1838–1840.
29 Egashira K, Zhao Q, Kataoka C, Ohtani K, Usui M, Charo IF, *et al.* Importance of monocyte chemoattractant protein-1 pathway in neointimal hyperplasia after periarterial injury in mice and monkeys. *Circ Res* 2002; **90**:1167–1172.
30 Horvath C, Welt FG, Nedelman M, Rao P, Rogers C. Targeting CCR2 or CD18 inhibits experimental in-stent restenosis in primates: inhibitory potential depends on type of injury and leukocytes targeted. *Circ Res* 2002; **90**:488–494.
31 Denger S, Jahn L, Wende P, Watson L, Gerber SH, Kubler W, Kreuzer J. Expression of monocyte chemoattractant protein-1 cDNA in vascular smooth muscle cells: induction of the synthetic phenotype: a possible clue to SMC differentiation in the process of atherogenesis. *Atherosclerosis* 1999; **144**:15–23.
32 Selzman CH, Miller SA, Zimmerman MA, Gamboni-Robertson F, Harken AH, Banerjee A. Monocyte chemotactic protein-1 directly induces human vascular smooth muscle proliferation. *Am J Physiol Heart Circ Physiol* 2002; **283**:H1455–H1461.
33 Viedt C, Vogel J, Athanasiou T, Shen W, Orth SR, Kubler W, Kreuzer J. Monocyte chemoattractant protein-1 induces proliferation and interleukin-6 production in human smooth muscle cells by differential activation of nuclear factor-kappaB and activator protein-1. *Arterioscler Thromb Vasc Biol* 2002; **22**:914–920.

Am J Physiol Heart Circ Physiol 291: H2237–H2245, 2006.
First published July 14, 2006; doi:10.1152/ajpheart.00427.2006.

Overexpression of glutathione peroxidase attenuates myocardial remodeling and preserves diastolic function in diabetic heart

Shouji Matsushima,[1] Shintaro Kinugawa,[2] Tomomi Ide,[1] Hidenori Matsusaka,[1] Naoki Inoue,[2] Yukihiro Ohta,[2] Takashi Yokota,[2] Kenji Sunagawa,[1] and Hiroyuki Tsutsui[2]

[1]*Department of Cardiovascular Medicine, Graduate School of Medical Sciences, Kyushu University, Fukuoka; and* [2]*Department of Cardiovascular Medicine, Hokkaido University Graduate School of Medicine, Sapporo, Japan*

Submitted 28 April 2006; accepted in final form 18 June 2006

Matsushima, Shouji, Shintaro Kinugawa, Tomomi Ide, Hidenori Matsusaka, Naoki Inoue, Yukihiro Ohta, Takashi Yokota, Kenji Sunagawa, and Hiroyuki Tsutsui. Overexpression of glutathione peroxidase attenuates myocardial remodeling and preserves diastolic function in diabetic heart. *Am J Physiol Heart Circ Physiol* 291: H2237–H2245, 2006. First published July 14, 2006; doi:10.1152/ajpheart.00427.2006.— Oxidative stress plays an important role in the structural and functional abnormalities of diabetic heart. Glutathione peroxidase (GSHPx) is a critical antioxidant enzyme that removes H_2O_2 in both the cytosol and mitochondia. We hypothesized that the overexpression of GSHPx gene could attenuate left ventricular (LV) remodeling in diabetes mellitus (DM). We induced DM by injection of streptozotocin (160 mg/kg ip) in male GSHPx transgenic mice (TG+DM) and nontransgenic wildtype littermates (WT+DM). GSHPx activity was higher in the hearts of TG mice compared with WT mice, with no significant changes in other antioxidant enzymes. LV thiobarbituric acid-reactive substances measured in TG+DM at 8 wk were significantly lower than those in WT+DM (58 ± 3 vs. 71 ± 5 nmol/g, $P < 0.05$). Heart rate and aortic blood pressure were comparable between groups. Systolic function was preserved normal in WT+DM and TG+DM mice. In contrast, diastolic function was impaired in WT+DM and was improved in TG+DM as assessed by the deceleration time of peak velocity of transmitral diastolic flow and the time needed for relaxation of 50% maximal LV pressure to baseline value (tau; 13.5 ± 1.2 vs. 8.9 ± 0.7 ms, $P < 0.01$). The TG+DM values were comparable with those of WT+Control (tau; 7.8 ± 0.2 ms). Improvement of LV diastolic function was accompanied by the attenuation of myocyte hypertrophy, interstitial fibrosis, and apoptosis. Overexpression of GSHPx gene ameliorated LV remodeling and diastolic dysfunction in DM. Therapies designed to interfere with oxidative stress might be beneficial to prevent cardiac abnormalities in DM.

oxidative stress; diabetes mellitus; heart failure; antioxidant; hypertrophy; glutathione peroxidase

DIABETES MELLITUS OFTEN LEADS to congestive heart failure, even in the absence of any other risk factors such as coronary artery disease or hypertension, suggesting that diabetes itself causes a specific form of cardiomyopathic state, independent of vascular complications (3). Specifically, diastolic dysfunction has been regarded as a hemodynamic hallmark seen in diabetes and ultimately contributes to the development of heart failure (1, 21). Diabetes causes myocardial structural remodeling characterized by myocyte hypertrophy and apoptosis as well as interstitial fibrosis (7), which increases cardiac muscle stiffness and may contribute to impaired diastolic function. Although the features of diabetic heart disease have been well identified, its pathogenesis and, in particular, the mechanisms underlying myocardial remodeling process have not been fully elucidated.

The excess production of reactive oxygen species (ROS), resulting in oxidative stress, is widely considered to be a cause of tissue damage associated with diabetes (2, 23). Our previous studies have demonstrated that H_2O_2 and hydroxyl radical (·OH), generated via superoxide anion (O_2^-·), play an important role in the development and progression of myocardial remodeling in the pacing-induced heart failure as well as in the postinfarct heart failure model (10, 28). Furthermore, in vitro studies demonstrated that ROS could directly induce hypertrophy and apoptosis in cardiac myocytes (30). Therefore, oxidative stress may contribute to the development of myocardial remodeling seen in diabetes (27). In fact, previous studies reported that antioxidants could attenuate myocardial damage in experimental diabetes (24, 36).

The first line of defense against ROS-mediated cardiac injury comprises several antioxidant enzymes including superoxide dismutase (SOD), catalase, and glutathione peroxidase (GSHPx). SOD, including mitochondrial Mn-SOD and cytosolic Cu/Zn-SOD, could provide antioxidant protection by inactivating O_2^-·, sparing nitric oxide from destruction, and preventing O_2^-· from forming more destructive ROS such as peroxynitrite and its reaction products, including ·OH. However, greater dismutation of O_2^-· by SOD results in an increase of H_2O_2. Therefore, among these antioxidants, GSHPx is an important enzyme that performs several vital functions (28). GSHPx not only functions by removing H_2O_2 formed after the SOD-catalyzed dismutation reaction, but also detoxifies the lipid hydroperoxides. In several in vitro studies, GSHPx alone was demonstrated to confer greater protection against oxidative damage than either SOD or catalase or the combination of SOD and catalase (31). The great efficiency of GSHPx as an antioxidant may be attributable to the fact that it is located in both the cytosol and the mitochondrial matrix and that it can utilize lipid peroxides as well as H_2O_2 for substrates. These beneficial characteristics make GSHPx an important candidate for therapy against myocardial remodeling and failure due to increased ROS production. Our previous studies have demonstrated that GSHPx overexpression can attenuate oxidative stress as well as postinfarct cardiac remodeling and failure (28). Therefore, the purpose of this study was to determine whether overexpression of GSHPx could attenuate the structural remodeling and func-

Address for reprint requests and other correspondence: H. Tsutsui, Dept. of Cardiovascular Medicine, Hokkaido Univ. Graduate School of Medicine, Kita-15, Nishi-7, Kita-ku, Sapporo 060-8638, Japan (e-mail: htsutsui@med.hokudai.ac.jp).

The costs of publication of this article were defrayed in part by the payment of page charges. The article must therefore be hereby marked "*advertisement*" in accordance with 18 U.S.C. Section 1734 solely to indicate this fact.

tional decline in the hearts with diabetes using GSHPx transgenic (TG) mice (20).

MATERIALS AND METHODS

TG mice. This study was approved by our Institutional Animal Research Committee and conformed to the animal care guidelines of the American Physiological Society. We used the progeny of heterozygous breeding pairs of the C57BL/6×CBA/J hybrid mice with the overexpression of the human GSHPx1 gene (20). The coding region of the human GSHPx gene was inserted into the unique *Bam*HI site of the pHMG cassette vector. To generate TG mice, *Not*I fragments of recombinant plasmids were microinjected into the pronuclei of the C57BL/6×CBA/J hybrid. Mouse strain 23 (containing 200 copies of the human GSHPx gene) was used for further studies. To obtain TG animals and their normal littermates for experiments, TG founders (kindly provided by Drs. Oleg Mirochnitchenko and Masayori Inouye, University of Medicine and Dentistry of New Jersey) were bred with (C57BL/6 × CBA/J)F_1 mice. Tail clips and a PCR protocol to confirm the genotype were performed by a group of investigators.

Induction of diabetes. Diabetes was induced in 8-wk-old male mice, weighing 26–32 g, by injection with streptozotocin (STZ; 160 mg/kg ip). Tail vein blood glucose samples were measured 5 days after injection to insure induction of diabetes. As a control, vehicle (0.1 mol/l citrate buffer, pH 4.5) was injected in wild-type (WT) and TG mice. This assignment procedure was performed with the use of numeric codes to identify the animals.

Echocardiographic and hemodynamic measurements. After 8 wk of injection, echocardiographic studies were performed under light anesthesia with tribromoethanol-amylene hydrate (Avertin; 2.5% wt/vol, 8 μl/g ip) and spontaneous respiration. Two-dimensional targeted M-mode tracings were recorded at a paper speed of 50 mm/s (28).

To assess diastolic cardiac function, two-dimensional guided Doppler flow measurements of mitral inflow were obtained. Mitral inflow velocities were recorded only after extensive scanning from multiple vantage points to ensure that the maximal velocity was obtained. In most situations, this was an apical window corresponding to an "off-axis" apical window (displaced toward the parasternal window). Early and late mitral inflow velocity (E wave and A wave, respectively) and E wave deceleration time were measured from the Doppler recordings in the standard fashion, and the E-to-A ratio was calculated (17).

Under the same anesthesia with Avertin, a 1.4-Fr micromanometer-tipped catheter (Millar Instruments) was inserted into the right carotid artery and then advanced into the left ventricle (LV) to measure LV pressures. The following indexes of cardiac performance were measured and averaged from three consecutive beats; LV systolic pressure, LV end-diastolic pressure (EDP), the maximum and minimum values of the first derivative of LV pressure ($LVdP/dt_{max}$ and $LVdP/dt_{min}$, respectively), and the time needed for relaxation of 50% maximal LV pressure to baseline value (tau). One subset of investigators, who were not informed of the experimental groups, performed in vivo LV function studies.

Plasma glucose. After completion of the cardiac function measurements performed after 2 h of fasting, blood samples were collected for the determination of plasma glucose.

Myocardial histopathology. After in vivo studies, the heart was excised and dissected into the right and left ventricles, including the septum. The LV was cut into three transverse sections: apex, middle ring, and base. From the middle ring, 5-μm sections were cut and stained with Masson's trichrome. Myocyte cross-sectional area was determined by quantitative morphometry of tissue sections from the mid-LV (28). Collagen distribution was also determined by using picrosirius red (0.1% Sirius Red F3BA in picric acid)-stained sections. Slides were left in 0.2% phosphomolybdic acid for 5 min, washed, and left in picrosirius red for 90 min and then in 1 mmol/l HCl for 2 min and 70% ethanol for 45 s.

To detect apoptosis, tissue sections from the mid-LV were stained with terminal deoxynucleotidyl transferase-mediated dUTP nick end-labeling (TUNEL) staining. The number of TUNEL-positive cardiac myocyte nuclei was counted, and the data were normalized per 10^5 total nuclei identified by hematoxylin-positive staining in the same sections (28).

Antioxidant enzyme activities and lipid peroxidation. The enzymatic activities of GSHPx, catalase, and total SOD were measured in the LV according to the methods described previously (28).

Lipid peroxidation is a major biochemical consequence of ROS attack on biological tissue. We therefore determined the degree of lipid peroxidation in the myocardial tissue through biochemical assay of thiobarbituric acid reactive substances (TBARS) (28). In brief, LV myocardial tissue was homogenized (10% wt/vol) in 1.15% KCl solution (pH 7.4). The homogenate was mixed with 0.4% SDS, 7.5% acetic acid adjusted to pH 3.5 with NaOH, and 0.3% thiobarbituric acid. Butylated hydroxytoluene (0.01%) was added to the assay mixture to prevent autoxidation of the sample. The mixture was kept at 5°C for 60 min and was heated at 100°C for 60 min. After cooling, the mixture was extracted with distilled water and *n*-butanol-pyridine (15:1, vol/vol) and centrifuged at 1,600 *g* for 10 min. The absorbance of the organic phase was measured at 532 nm. The amount of TBARS was determined by absorbance with the molecular extinction coefficient of 156,000 (and expressed as μmol/g wet wt).

To further assess the lipid peroxidation by histochemical analysis, LV myocardial sections were immunolabeled with an antibody raised against 4-hydroxy-2-nonenal (HNE)-modified protein, an aldehydic byproduct of lipid peroxidation (10). In brief, paraffin-embedded tissue sections (3-μm thick) were deparaffinized with xylene and refixed with Bouin's solution for 20 min and immersed in 70, 90, and 100% ethanol to remove picric acid. To inhibit endogenous peroxidase, the sections were incubated with 0.3% H_2O_2 in methanol for 30 min. After a rinsing in 0.01 mol/l PBS, the sections were incubated with normal goat serum (diluted to 1:10) to inhibit nonspecific binding of antibodies. The sections were further incubated with polyclonal antiserum raised against an HNE-modified histidyl peptide (Gly3-His-Gly3) conjugated with keyhole-limpet hemocyanin. After a rinsing with 0.01 mol/l PBS, the sections were incubated with biotin-labeled mouse anti-mouse IgG antiserum (diluted 1:100; Nihonyushi N213220) for 60 min and then with avidin-biotin complex (Vectastain ABC kit; 1:100) for 60 min. After a rinsing, the sections were finally incubated with 0.02% 3,3′-diaminobenzidine and 0.03% H_2O_2 in deionized water for 6–9 min. As a negative control, the sections were also incubated with normal rabbit serum.

A morphometric analysis of HNE-positive myocardial area was performed with tissue sections stained with HNE. Each section was photographed under a microscope and magnified (final magnification, ×200). Three to four fields were randomly selected from one or two coronal sections in each animal. As a result, the HNE-positive areas were measured at approximately five to seven fields for each animal. Within each field, myocardial segments that stained positively with anti-HNE antibody were identified and were manually traced by use of a digitizing pad with a computer to calculate the traced area.

Matrix metalloproteinases, transforming growth factor-β, and connective tissue growth factor. We further determined the alterations of profibrotic mediators including matrix metalloproteinases (MMPs), transforming growth factor (TGF)-β, and connective tissue growth factor (CTGF) in this model.

First, the myocardial MMP levels, including MMP-2 and MMP-9, were determined in the LV using gelatin zymography (10). The LV myocardial samples were homogenized (~30-s bursts) in 1 ml of an ice-cold extraction buffer containing cacodylic acid (10 mmol/l), NaCl (0.15 mol/l), $ZnCl_2$ (20 mmol/l), NaN_3 (1.5 mmol/l), and 0.01% Triton X-100 (pH 5.0). The homogenate was then centrifuged (4°C, 10 min, 10,000 *g*), and the supernatant was decanted and saved on ice.

The pH levels of the samples were adjusted to 7.5 by use of Tris (1 mol/l). The final protein concentration of the myocardial extracts was determined using a standardized colorimetric assay. The extracted samples were then aliquoted and stored at −80°C until the time of assay. The myocardial extracts were then directly loaded onto electrophoretic gels (SDS-PAGE) containing 1 mg/ml gelatin under nonreducing conditions. The myocardial extracts at a final protein content of 5 μg were loaded onto the gels using a 3:1 sample buffer (10% SDS, 4% sucrose, 0.25 mol/l Tris-Cl, and 0.1% bromophenol blue, pH 6.8). The gels were run at 15 mA/gel through the stacking phase (4%) and at 20 mA/gel for the separating phase (10%), while the running buffer temperature was maintained at 4°C. After SDS-PAGE, the gels were washed twice in 2.5% Triton X-100 for 30 min each, rinsed in water, and incubated for 24 h in a substrate buffer at 37°C (50 mmol/l Tris·HCl, 5 mmol/l $CaCl_2$, and 0.02% NaN_3, pH 7.5). After incubation, the gels were stained with Coomassie brilliant blue R-250. The zymograms were digitized, and the size-fractionated bands, which indicated the MMP proteolytic levels, were measured by integrated optical density in a rectangular region of interest.

Next, the mRNA levels of myocardial MMPs including MMP-1, -2, -3, -8, and -9 as well as tissue inhibitors of MMPs (TIMPs) including TIMP-1, -2, -3, and -4 were determined by multiprobe ribonuclease protection assay (RPA RiboQuant, PharMingen). Each value was normalized to that of glyceraldehydes-3-phosphate dehydrogenase (GAPDH) in each template set as an internal control, followed by calculation as a ratio to WT+Control.

The expression level of genes including the TGF-β gene was determined by ribonuclease protection assay. The value of each hybridized probe was normalized to that of GAPDH in each template set as an internal control. CTGF protein levels were quantified by Western blot analysis using a specific antibody against recombinant mouse CTGF. To confirm the amount of loaded proteins, total proteins were also visualized by Coomassie brilliant blue staining. Within a given experiment, the densitometric values were normalized, using standards concurrently run within the same gel, and the value for each WT+diabetes mellitus (DM) or TG+DM was calculated as a ratio of WT+Control.

Statistical analysis. Data are expressed as means ± SE. Between-group comparison of means was performed by one-way ANOVA, followed by *t*-tests. The Bonferroni's correction was done for multiple comparisons of means. $P < 0.05$ was considered to be statistically significant.

RESULTS

Antioxidant enzymes and TBARS. The baseline differences in antioxidant enzyme activities between WT and TG mice were determined (Table 1). In TG mice, there was a significant increase in GSHPx activities in the LV. Importantly, catalase and SOD activities were not altered in the TG hearts, indicating no effects of GSHPx overexpression on other antioxidant enzymes. Similar results have been reported in the brain, liver, kidney, and lung obtained from the same series of mice (11, 22). The changes of antioxidant enzyme activities by the presence of diabetes were compared between WT and TG mice. GSHPx activities were comparable between WT+Control and WT+DM (Table 1). More importantly, as expected, GSHPx activities were significantly higher in TG+DM compared with WT+DM (Table 1). SOD and catalase activities were not altered in WT+DM or TG+DM compared with WT+Control.

Table 1. *Antioxidant enzymes*

	WT+Control (n = 9)	TG+Control (n = 9)	WT+DM (n = 9)	TG+DM (n = 9)
GSHPx, nmol·min^{-1}·mg protein^{-1}	44.9±2.5	68.1±5.0*†	45.6±3.1	68.8±8.3*†
Catalase, nmol/mg protein	67.8±7.5	89.5±15.4	64.4±7.0	90.0±10.1
Total SOD, U/mg protein	14.6±1.3	15.7±1.6	19.2±2.4	19.0±1.8

Values are means ± SE; n is number of mice. GSHPx, glutathione peroxidase; SOD, superoxide dismutase; WT, wildtype; TG, transgenic; DM, diabetes mellitus. *$P < 0.05$ vs. WT+Control. †$P < 0.05$ vs. WT+DM.

TBARS measured in the LV obtained from WT+DM tended to be greater compared with WT+DM, which, however, did not reach statistical significance ($P = 0.05$). Importantly, TBARS from TG+DM were significantly lower than those from WT+DM (Fig. 1*A*). In accordance with TBARS, an immunohistochemical analysis of HNE-modified protein revealed the lipid peroxides to be positively stained in myocytes from WT+DM mice, whereas only faint labeling was observed in the WT+Control, TG+Control, and TG+DM (Fig. 1*B*). The myocardial area stained positively with HNE was significantly smaller in TG+DM than in WT+DM.

Body weight and plasma glucose. There was no death in any group of mice. DM animals gained less body weight than control mice, which, however, did not differ between WT+DM and TG+DM (Table 2). At 5 days and 8 wk, DM mice had increased plasma glucose levels compared with control animals, which was not altered by GSHPx gene overexpression (Table 2).

Echocardiography and hemodynamics. The echocardiographic and hemodynamic data of mice at 8 wk are shown in Table 3. There was no significant difference in heart rate and aortic blood pressure among four groups of mice. Systolic function, as assessed by echocardiographic fractional shortening and $LVdP/dt_{max}$, was preserved as normal in both WT+DM and TG+DM mice. In contrast, diastolic function, as assessed by the deceleration time of peak velocity of transmitral diastolic flow (Dct) and the time needed for relaxation of 50% maximal LV pressure to baseline value (tau), was impaired in WT+DM, which was significantly attenuated in TG+DM (Table 3). $LVdP/dt_{min}$ tended to be decreased in WT+DM compared with WT+Control ($P = 0.05$) and increased in TG+DM compared with WT+DM ($P = 0.09$), both of which, however, did not reach statistical significance. LVEDP was slightly, but significantly, elevated in WT+DM, which was attenuated in TG+DM.

Myocardial histomorphometry and apoptosis. Increased cardiac myocyte size, indicating hypertrophy, was evident in WT+DM, and this increase was significantly attenuated in TG+DM (Fig. 2). Collagen volume fraction, indicating interstitial fibrosis, in the WT+DM group was greater than in the control groups (Fig. 2). These fibrotic changes in the heart were significantly reduced in the TG+DM group.

The number of TUNEL-positive cells in the LV from the TG+DM group was significantly decreased compared with the WT+DM group and held constant relative to the control groups (Fig. 3).

Myocardial MMPs, TGF-β, and CTGF. To further assess the alterations of profibrotic mediators to be involved in interstitial fibrosis, myocardial levels of MMPs, TGF-β, and CTGF were determined.

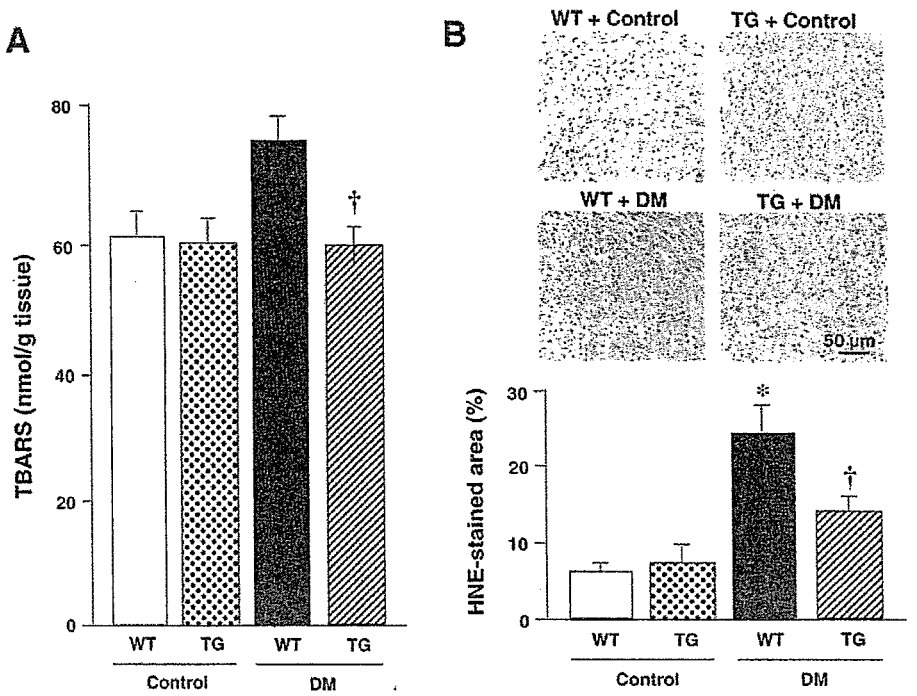

Fig. 1. *A*: lipid peroxidation as indicated by thiobarbituric acid reactive substances (TBARS) in the myocardial tissue from WT+Control, TG+Control, WT+DM, and TG+DM hearts (n = 14 for each). WT, wild-type; TG, transgenic; DM, diabetes mellitus. Each assay was performed in triplicate. Values are means ± SE. †$P < 0.05$, difference from WT+DM value. *B*: representative immunohistochemical micrograph analysis and summary data for 4-hydroxy-2-nonenal (HNE)-modified histidine peptide in the myocardial tissue sections from WT+Control, TG+Control, WT+DM, and TG+DM mice (n = 3 for each). *$P < 0.05$, difference from the WT+Control value. †$P < 0.05$, difference from the WT+DM value.

Myocardial MMP-2 zymographic levels were increased in WT+DM, and this increase was significantly attenuated in TG+DM (Fig. 4). MMP-9 protein levels, although they were faint, were not altered in WT+DM or TG+DM. Other MMPs including MMP-1, -3, and -8 and TIMPs including TIMP-1, -2, -3, and -4 were not altered in the hearts from four groups of mice (Fig. 5).

Myocardial TGF-β gene expression was increased in WT+DM, which was significantly attenuated in TG+DM (Fig. 6*A*). In parallel with TGF-β, CTGF protein levels were increased in WT+DM, which, however, was not attenuated in TG+DM (Fig. 6*B*).

DISCUSSION

The present study demonstrated that overexpression of GSHPx attenuated oxidative stress in the myocardial tissue and concurrently improved LV diastolic function as well as reduced myocyte hypertrophy, apoptosis, and interstitial fibrosis. Although the beneficial effects of various antioxidants on the diabetic heart have been demonstrated already by previous studies (6, 24, 36), the present study specifically provided direct evidence for the protective role of GSHPx against myocardial remodeling and dysfunction in this disease state.

Table 2. *Body weight and blood glucose data*

	WT+Control (n = 16)	TG+Control (n = 14)	WT+DM (n = 13)	TG+DM (n = 13)
Body weight, g	33.5±1.1	31.7±1.0	27.2±0.7‡	27.4±0.7‡
Glucose, mg/dl (5 days after injection)	119±5	114±4	332±24‡	350±36‡
Glucose, mg/dl (8 wk after injection)	127±8	125±6	431±36‡	420±7‡

Values are means ± SE; n is number of mice. ‡$P < 0.01$ vs. WT+Control.

The most effective way to evaluate the contribution of the specific antioxidant and obtain the direct evidence for a role of oxidative stress is through gene manipulation instead of the administration of antioxidants. Therefore, the novel finding of the present study from the point of view of understanding the pathophysiology and treatment of maladaptive myocardial remodeling in response to diabetes mellitus is that H_2O_2 is critically involved in this disease process and may be a potential therapeutic target. Although the present study does not support the notion that the alterations in GSHPx are involved in oxidative stress in the diabetic heart, the overexpression of this gene can prevent the increase of oxidative stress as well as cardiac remodeling in diabetes mellitus.

A growing body of evidence suggests that the production of ROS is increased in the diabetic heart (14). Specifically, ROS are produced within the mitochondria of these hearts (15, 23). Furthermore, antioxidants have been shown to prevent the structural and functional alterations of the diabetes heart (6, 24, 36). Therefore, the present study not only extends the previous observation that employed antioxidants but also reveals the major role of ROS in the pathophysiology of cardiac remodeling associated with diabetes.

GSHPx is a key antioxidant that catalyzes the reduction of H_2O_2 and hydroperoxides. It not only scavenges H_2O_2 but also prevents the formation of other more toxic radicals such as ·OH. GSHPx possesses a higher affinity for H_2O_2 than catalase. Furthermore, it is present in relatively high amounts within the heart, especially in the cytosolic and mitochondrial compartments (18). These lines of evidence imply the primary importance of GSHPx as a defense mechanism within the heart compared with catalase. Moreover, GSHPx is expected to exert greater protective effects against oxidative damage than SOD because greater dismutation of O_2^-· by SOD may result in an increase of H_2O_2. Therefore, compared with SOD or catalase,

Table 3. *Echocardiographic and hemodynamic data*

	WT+Control	TG+Control	WT+DM	TG+DM
		Echocardiographic data		
n	16	14	13	13
Heart rate, beats/min	466±12	448±7	417±6	420±7
LV EDD, mm	3.7±0.1	3.6±0.1	3.5±0.1	3.5±0.1
LV ESD, mm	2.4±0.1	2.3±0.1	2.3±0.1	2.2±0.1
Fractional shortening, %	35.1±0.5	35.5±0.8	34.1±0.7	36.1±0.6
IVS thickness, mm	0.71±0.02	0.70±0.02	0.68±0.02	0.68±0.02
PW thickness, mm	0.74±0.02	0.74±0.03	0.72±0.02	0.73±0.02
E/A ratio	1.49±0.06	1.60±0.12	1.28±0.06	1.31±0.07
Dct, ms	33.6±0.6	34.6±1.3	45.3±1.6‡	37.5±0.9§
		Hemodynamic data		
n	13	13	13	13
Heart rate, beats/min	438±12	439±13	413±4	431±17
Systolic aortic pressure, mmHg	98±3	101±4	102±5	101±6
Diastolic aortic pressure, mmHg	66±3	72±4	72±4	71±5
Mean aortic pressure, mmHg	76±3	82±4	83±5	82±6
LVEDP, mmHg	1.7±0.2	2.2±0.4	4.4±0.6‡	1.2±0.4§
$LVdP/dt_{max}$, mmHg/s	7,376±912	9,816±758	5,742±665	8,646±649
$LVdP/dt_{min}$, mmHg/s	6,996±822	7,052±700	4,458±330	6.036±547
Tau, ms	7.8±0.2	8.2±0.4	13.5±1.2‡	8.9±0.7§

Values are means ± SE; *n*, number of mice. LV, left ventricular; EDD, end-diastolic diameter; ESD, end-systolic diameter; IVS, interventricular septal; PW, posterior wall; E, peak velocity of early mitral flow; A, peak velocity of late mitral flow; Dct, deceleration time; EDP, end-diastolic pressure; dP/d*t*, change in pressure over time; tau, time needed for relaxation of 50% maximal LV pressure to baseline value. ‡$P < 0.01$ vs. WT+Control. §$P < 0.01$ vs. WT+DM.

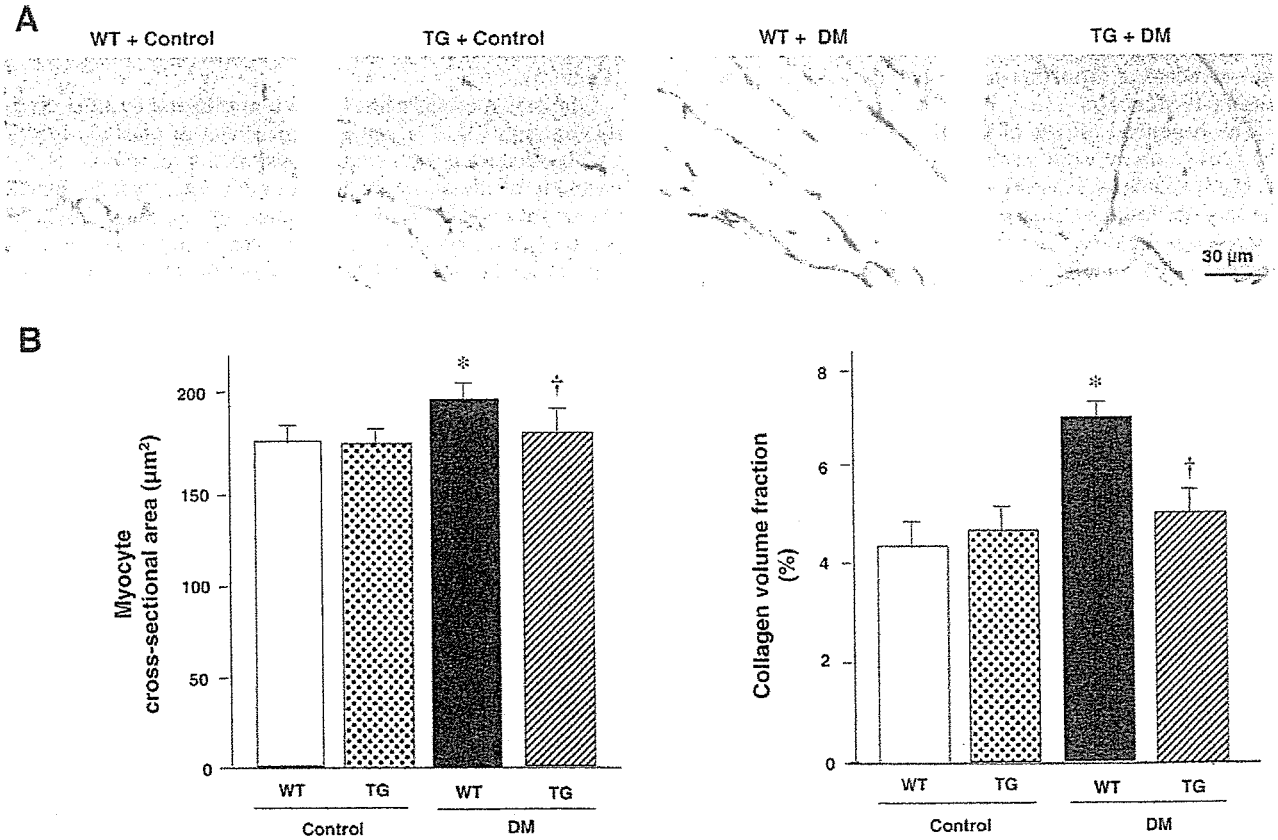

Fig. 2. *A*: representative photomicrographs of Masson's trichrome-stained left ventricular (LV) cross section obtained from 4 groups of mice. *B*: summary data for myocyte cross-sectional area and collagen volume fraction in WT+Control ($n = 11$), TG+Control ($n = 8$), WT+DM ($n = 12$), and TG+DM ($n = 11$) mice. Values are means ± SE. *$P < 0.05$, difference from the WT+Control value. †$P < 0.05$, difference from the WT+DM value.

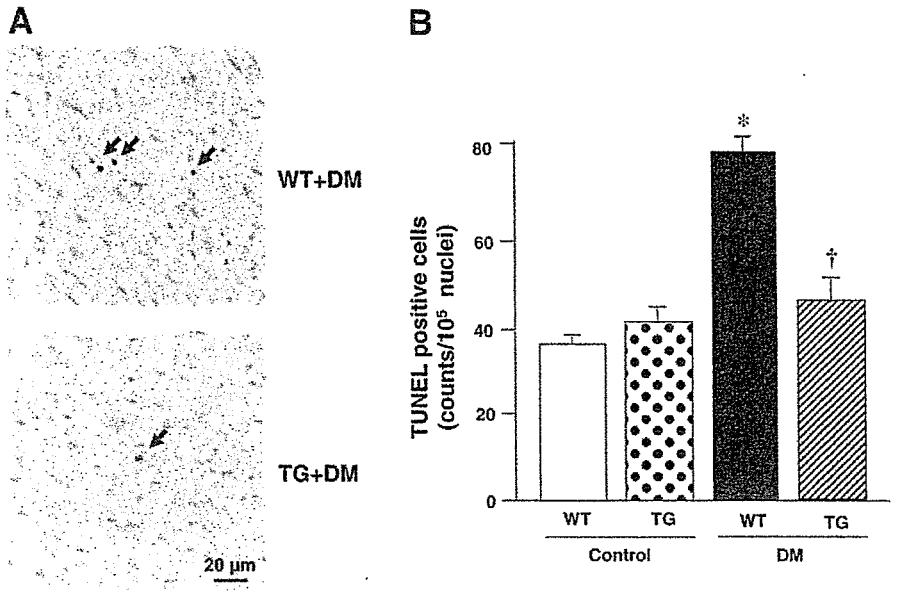

Fig. 3. *A*: representative photomicrographs of TUNEL-stained cells (arrows) within LV cross-sections obtained from WT+DM and TG+DM mice. *B*: no. of TUNEL-positive myocytes in the LV from WT+Control, TG+Control, WT+DM, and TG+DM mice (n = 5 each). Values are means ± SE. *P < 0.05, difference from the WT+Control value. †P < 0.05, difference from the WT+DM value.

GSHPx is thought to be more effective in protecting cells, tissues, and organs against oxidative damage (5, 31). In fact, our previous studies demonstrated that the mice with GSHPx gene overexpression were more resistant to myocardial oxidative stress as well as remodeling and failure after myocardial infarction (28). Thus the present study extends the previous observation by demonstrating that they can attenuate not only post-myocardial infarction failure but also diabetes-associated cardiac dysfunction.

The beneficial effects of GSHPx overexpression shown in the present study were primarily due to its scavenging action on H_2O_2 (Table 1). However, we could not completely exclude the possibility that altered expression of other antioxidant enzymes is involved. LV total SOD activities tended to be higher in WT and TG mice with diabetes; however, they did not reach statistical significance. Total SOD may be induced in the presence of DM, even though its pathophysiological significance remains uncertain. In addition, GSHPx TG mice tended to have higher levels of catalase (Table 1), which did not reach statistical significance. Nevertheless, we could not exclude the possibility that there were synergistic antioxidant effects between GSHPx and catalase against H_2O_2, because both possess a high affinity for H_2O_2. Furthermore, the beneficial effects of GSHPx overexpression were not due to the effects on diabetes itself, because body weight and plasma glucose levels were comparable between WT+DM and TG+DM mice (Table 2). Importantly, the effects were not attributable to those of GSHPx overexpression on hemodynamics, because blood pressure and heart rate were not altered (Table 3).

Diabetes mellitus causes both diastolic and systolic cardiac dysfunction (27, 37), but an impairment of diastolic function usually occurs before systolic dysfunction develops. The impairment of diastolic function despite normal systolic function is thought to result from an increased myocardial stiffness. The present study has clearly demonstrated that the attenuation of myocardial oxidative stress by GSHPx overexpression (Fig. 1) is associated with the attenuation of diastolic dysfunction (Table 3), myocyte hypertrophy, and interstitial fibrosis (Fig. 2) in diabetes. Previous studies have demonstrated that diabetes induced by STZ leads to an increased collagen deposition (25), resulting in an increased myocardial stiffness and a decrease in LV compliance (19, 24). Although we did not directly assess the diastolic function by using the stress-

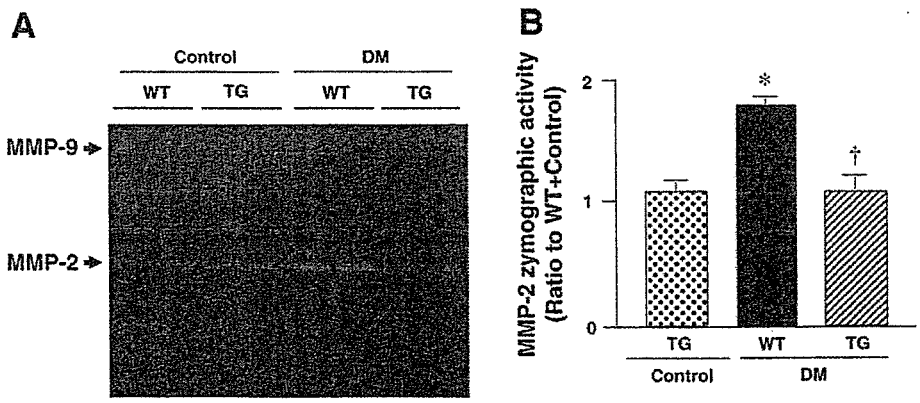

Fig. 4. *A*: representative gelation zymography indicating myocardial matrix metalloproteinase (MMP)-2 activity in WT+Control, TG+Control, WT+DM, and TG+DM mice. *B*: summary data for myocardial MMP-2 activity in 4 groups of mice (n = 9 each). Data were expressed as the ratio to WT+Control values concurrently run on the same gel. Values are means ± SE. *P < 0.05, difference from the WT+Control value. †P <0.05, difference from the WT+DM value.

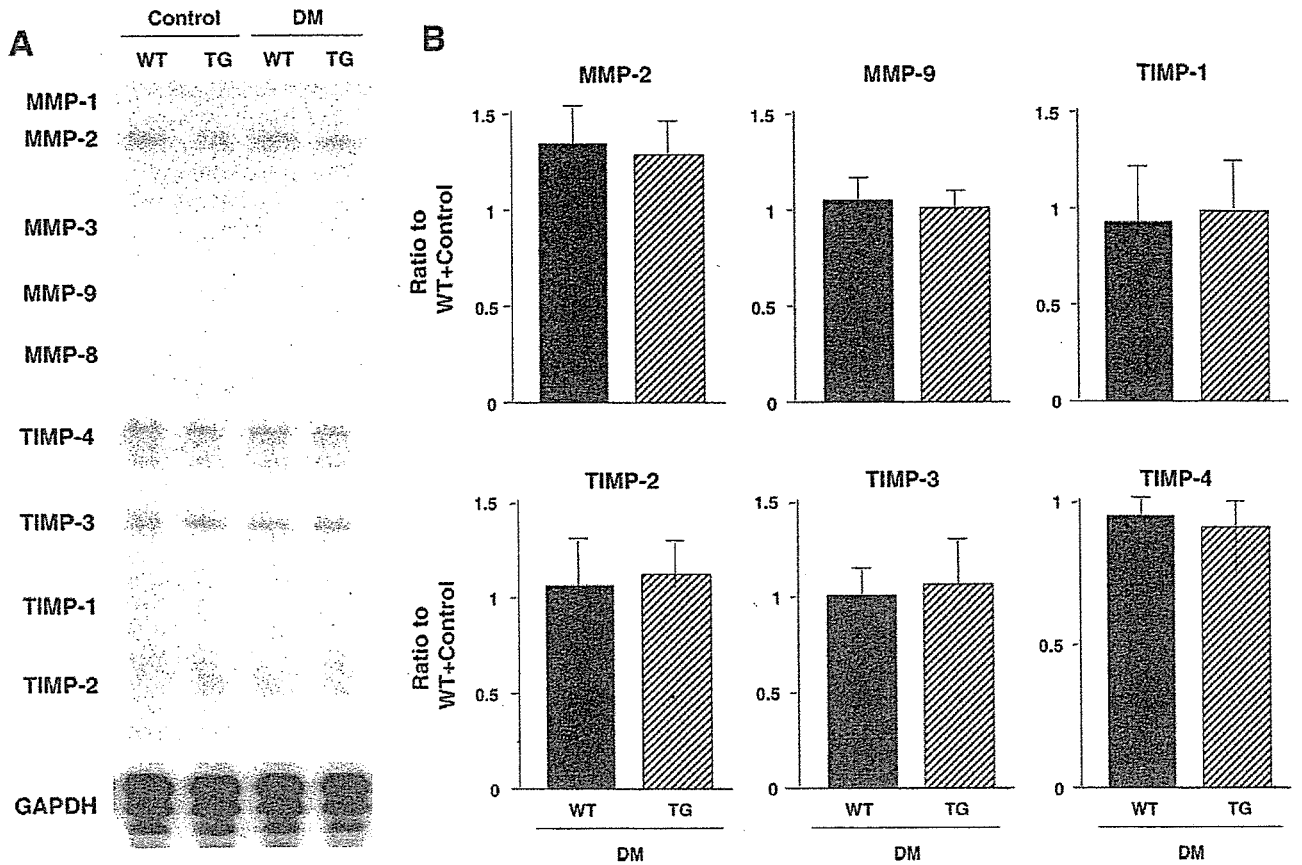

Fig. 5. *A*: representative image of myocardial gene expression of MMPs/tissue inhibitors of MMPs (TIMP). *B*: densitometric analysis of MMP and TIMP gene expression from WT+DM (n = 4) and TG+DM mice (n = 4). Each value was normalized to that of GAPDH in each template set as an internal control and expressed as the ratio to WT+Control (n = 4). Values are means ± SE.

strain relations and therefore could not comment on the contribution of myocardial stiffness to LV function in the present study, the decline in myocardial fibrosis in TG+DM mice can well be considered to contribute to the physiological improvement of diastolic properties in these mice. In fact, prior studies have generally shown an association between increased cardiac fibrosis and diastolic chamber stiffening (35).

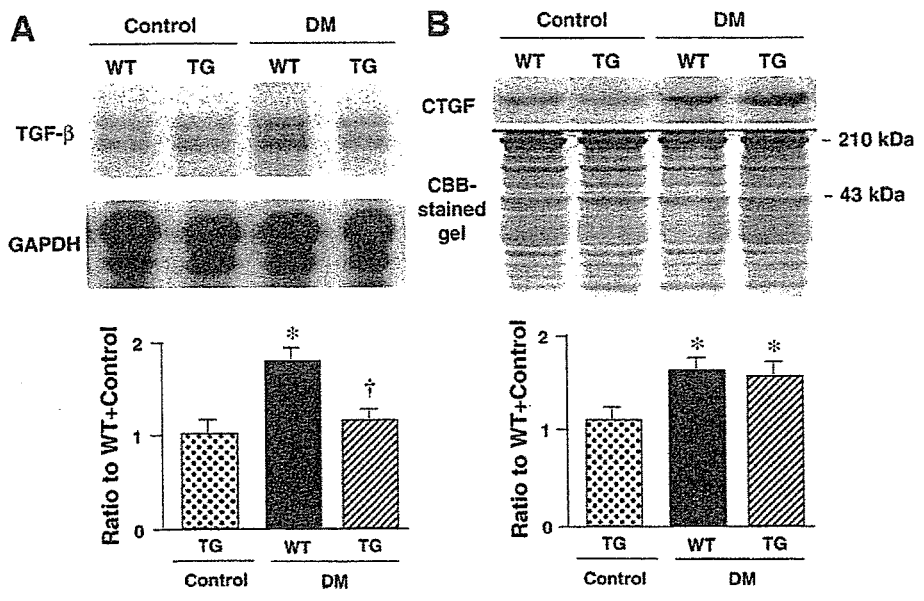

Fig. 6. Myocardial transforming growth factor (TGF)-β (*A*) and connective tissue growth factor (CTGF; *B*) levels in WT+Control, TG+Control, WT+DM, and TG+DM mice (n = 6 each). Data were expressed as the ratio to WT+Control values concurrently run on the same gel. Values are means ± SE. *P < 0.05, difference from the WT+Control value. †P <0.05, difference from the WT+DM value.

The present results are consistent with previous studies demonstrating that ROS are involved in the structural alterations of the extracellular matrix collagens. The increase in collagens and myocardial stiffness in STZ-induced diabetic rats was prevented by treatment with aminoguanidine (24) and antioxidants (26, 34).

There may be several factors whereby oxidative stress contributes to myocardial remodeling in diabetes. First, oxidative stress is involved in cardiac myocyte hypertrophy and apoptosis (Figs. 2 and 3). It has been demonstrated that a subtle increase in ROS caused by partial inhibition of SOD results in hypertrophy and apoptosis in isolated cardiac myocytes (30), both of which are thought to contribute to diabetic myocardial damage. Specifically, recent studies show that the incidence of apoptosis is increased in the diabetic heart (4, 7), which may cause loss of contractile myocytes, compensatory hypertrophy of myocytes, and interstitial infibrosis (6). Myocyte necrosis also may be involved in the increased fibrosis from the diabetic heart. Second, oxidative stress induces the activation of MMP-2 seen in diabetes (Fig. 4). Our previous studies have demonstrated that MMP-2 activation plays an important role in the pathophysiology of cardiac remodeling (16). Moreover, MMPs have been shown to be activated by ROS in cardiac fibroblasts (29). On the basis of these findings, it is conceivable to hypothesize that increased ROS contribute to the activation of MMP and thus to the development of interstitial fibrosis in diabetes. Third, a possible role for growth factors in diabetes-related end-organ complications is increasingly being recognized. TGF-β and CTGF can induce the production of collagen and fibronectin from cardiac fibroblasts and myocytes, and increased expression of both factors has been documented in the diabetic heart (12, 32). CTGF has a unique TGF-β response element in its promoter region (8) and acts downstream of TGF-β. The present study demonstrated that the attenuation of cardiac fibrosis by GSHPx overexpression was associated with the decrease in TGF-β expression, but not with CTGF, suggesting that TGF-β mainly contributed to cardiac fibrosis in this model. Nevertheless, we could not completely exclude the contribution of other growth factors such as VEGF, FGF, or PDGF in our model.

Approximately 20–40% of patients with heart failure have preserved systolic function and are thought to have an impairment of diastolic function as the primary mechanism leading to symptomatic heart failure (33). Diabetes is recognized as one of the major risk factors associated with diastolic heart failure (13). Despite the high prevalence of diabetes among patients with this type of heart failure, the treatment of diastolic heart failure remains empirical (9). There are currently few clinical data to support the efficacy of any particular class of drugs for diastolic heart failure. Therefore, the present study should help clarify the potential that antioxidants may play in the treatment of diastolic heart failure.

There are several limitations to be acknowledged in this study. First, the echocardiographic assessment of LV diastolic function in mice is somewhat difficult. However, intra- and interobserver variabilities of our echocardiographic measurements were small, and measurements were highly reproducible. Therefore, our technique was capable of noninvasively assessing the LV structure and function in mice. Second, the relationships between cardiac function and structural alterations were analyzed only at 8 wk after the induction of diabetes. Longer follow-up must be performed to establish whether cardiac remodeling including myocyte hypertrophy, interstitial fibrosis, and apoptosis due to hyperglycemia may eventually lead to clinical heart failure in diabetes. Third, we employed myocyte cross-sectional area as an index of myocyte hypertrophy. Although this has been commonly used, we need to be cautious in interpreting these data, because increased myocyte cross-sectional area is not equivalent to myocyte hypertrophy, and the length of the cell is an equally important determinant of myocyte volume.

In conclusion, GSHPx overexpression inhibited the development of LV remodeling and diastolic dysfunction associated with diabetes. These beneficial effects of GSHPx were associated with the attenuation of myocyte hypertrophy, apoptosis, and interstitial fibrosis. Therapies designed to interfere with oxidative stress could be beneficial to prevent diabetic heart disease.

ACKNOWLEDGMENTS

A part of this study was conducted in Kyushu University Station for Collaborative Research I and II. We thank Drs. Oleg Mirochnitchenko and Masayori Inouye of University of Medicine and Dentistry of New Jersey-Robert Wood Johnson Medical School for providing us the original breeding pairs of GSHPx TG mice.

GRANTS

This study was supported in part by grants from the Ministry of Education, Science and Culture, Japan (nos. 12670676, 14370230, 17390223, and 17659223).

REFERENCES

1. **Abe T, Ohga Y, Tabayashi N, Kobayashi S, Sakata S, Misawa H, Tsuji T, Kohzuki H, Suga H, Taniguchi S, and Takaki M.** Left ventricular diastolic dysfunction in type 2 diabetes mellitus model rats. *Am J Physiol Heart Circ Physiol* 282: H138–H148, 2002.
2. **Baynes JW.** Role of oxidative stress in development of complications in diabetes. *Diabetes* 40: 405–412, 1991.
3. **Beckman JA, Creager MA, and Libby P.** Diabetes and atherosclerosis: epidemiology, pathophysiology, and management. *JAMA* 287: 2570–2581, 2002.
4. **Cai L, Li W, Wang G, Guo L, Jiang Y, and Kang YJ.** Hyperglycemia-induced apoptosis in mouse myocardium: mitochondrial cytochrome C-mediated caspase-3 activation pathway. *Diabetes* 51: 1938–1948, 2002.
5. **Cohen G and Hochstein P.** Glutathione peroxidase: the primary agent for the elimination of hydrogen peroxide in erythrocytes. *Biochemistry* 2: 1420–1428, 1963.
6. **Fiordaliso F, Bianchi R, Staszewsky L, Cuccovillo I, Doni M, Laragione T, Salio M, Savino C, Melucci S, Santangelo F, Scanziani E, Masson S, Ghezzi P, and Latini R.** Antioxidant treatment attenuates hyperglycemia-induced cardiomyocyte death in rats. *J Mol Cell Cardiol* 37: 959–968, 2004.
7. **Fiordaliso F, Li B, Latini R, Sonnenblick EH, Anversa P, Leri A, and Kajstura J.** Myocyte death in streptozotocin-induced diabetes in rats in angiotensin II- dependent. *Lab Invest* 80: 513–527, 2000.
8. **Grotendorst GR, Okochi H, and Hayashi N.** A novel transforming growth factor beta response element controls the expression of the connective tissue growth factor gene. *Cell Growth Differ* 7: 469–480, 1996.
9. **Hunt SA, Baker DW, Chin MH, Cinquegrani MP, Feldman AM, Francis GS, Ganiats TG, Goldstein S, Gregoratos G, Jessup ML, Noble RJ, Packer M, Silver MA, Stevenson LW, Gibbons RJ, Antman EM, Alpert JS, Faxon DP, Fuster V, Jacobs AK, Hiratzka LF, Russell RO, and Smith SC Jr; American College of Cardiology/American Heart Association Task Force on Practice Guidelines (Committee to Revise the 1995 Guidelines for the Evaluation and Management of Heart Failure); International Society for Heart and Lung Transplantation; Heart Failure Society of America.** ACC/AHA Guidelines for the Evaluation and Management of Chronic Heart Failure in the Adult: Executive Summary A Report of the American College of Cardiology/American Heart Association Task Force on Practice Guidelines (Commit-

tee to Revise the 1995 Guidelines for the Evaluation and Management of Heart Failure): Developed in Collaboration With the International Society for Heart and Lung Transplantation; Endorsed by the Heart Failure Society of America. *Circulation* 104: 2996–3007, 2001.

10. **Ide T, Tsutsui H, Kinugawa S, Suematsu N, Hayashidani S, Ichikawa K, Utsumi H, Machida Y, Egashira K, and Takeshita A.** Direct evidence for increased hydroxyl radicals originating from superoxide in the failing myocardium. *Circ Res* 86: 152–157, 2000.
11. **Ishibashi N, Weisbrot-Lefkowitz M, Reuhl K, Inouye M, and Mirochnitchenko O.** Modulation of chemokine expression during ischemia/reperfusion in transgenic mice overproducing human glutathione peroxidases. *J Immunol* 163: 5666–5677, 1999.
12. **Jesmin S, Sakuma I, Hattori Y, Fujii S, and Kitabatake A.** Long-acting calcium channel blocker benidipine suppresses expression of angiogenic growth factors and prevents cardiac remodelling in a Type II diabetic rat model. *Diabetologia* 45: 402–415, 2002.
13. **Jessup M and Brozena S.** Heart failure. *N Engl J Med* 348: 2007–2018, 2003.
14. **Kakkar R, Kalra J, Mantha SV, and Prasad K.** Lipid peroxidation and activity of antioxidant enzymes in diabetic rats. *Mol Cell Biochem* 151: 113–119, 1995.
15. **Kanazawa A, Nishio Y, Kashiwagi A, Inagaki H, Kikkawa R, and Horiike K.** Reduced activity of mtTFA decreases the transcription in mitochondria isolated from diabetic rat heart. *Am J Physiol Endocrinol Metab* 282: E778–E785, 2002.
16. **Kinugawa S, Tsutsui H, Hayashidani S, Ide T, Suematsu N, Satoh S, Utsumi H, and Takeshita A.** Treatment with dimethylthiourea prevents left ventricular remodeling and failure after experimental myocardial infarction in mice: role of oxidative stress. *Circ Res* 87: 392–398, 2000.
17. **Knollmann BC, Blatt SA, Horton K, de Freitas F, Miller T, Bell M, Housmans PR, Weissman NJ, Morad M, and Potter JD.** Inotropic stimulation induces cardiac dysfunction in transgenic mice expressing a troponin T (I79N) mutation linked to familial hypertrophic cardiomyopathy. *J Biol Chem* 276: 10039–10048, 2001.
18. **Le CT, Hollaar L, van der Valk EJ, and van der Laarse A.** Buthionine sulfoximine reduces the protective capacity of myocytes to withstand peroxide-derived free radical attack. *J Mol Cell Cardiol* 25: 519–528, 1993.
19. **Litwin SE, Raya TE, Anderson PG, Daugherty S, and Goldman S.** Abnormal cardiac function in the streptozotocin-diabetic rat. Changes in active and passive properties of the left ventricle. *J Clin Invest* 86: 481–488, 1990.
20. **Mirochnitchenko O, Palnitkar U, Philbert M, and Inouye M.** Thermosensitive phenotype of transgenic mice overproducing human glutathione peroxidases. *Proc Natl Acad Sci USA* 92: 8120–8124, 1995.
21. **Mizushige K, Yao L, Noma T, Kiyomoto H, Yu Y, Hosomi N, Ohmori K, and Matsuo H.** Alteration in left ventricular diastolic filling and accumulation of myocardial collagen at insulin-resistant prediabetic stage of a type II diabetic rat model. *Circulation* 101: 899–907, 2000.
22. **Nakatani T, Inouye M, and Mirochnitchenko O.** Overexpression of antioxidant enzymes in transgenic mice decreases cellular ploidy during liver regeneration. *Exp Cell Res* 236: 137–146, 1997.
23. **Nishikawa T, Edelstein D, Du XL, Yamagishi S, Matsumura T, Kaneda Y, Yorek MA, Beebe D, Oates PJ, Hammes HP, Giardino I, and Brownlee M.** Normalizing mitochondrial superoxide production blocks three pathways of hyperglycaemic damage. *Nature* 404: 787–790, 2000.
24. **Norton GR, Candy G, and Woodiwiss AJ.** Aminoguanidine prevents the decreased myocardial compliance produced by streptozotocin-induced diabetes mellitus in rats. *Circulation* 93: 1905–1912, 1996.
25. **Riva E, Andreoni G, Bianchi R, Latini R, Luvara G, Jeremic G, Traquandi C, and Tuccinardi L.** Changes in diastolic function and collagen content in normotensive and hypertensive rats with long-term streptozotocin-induced diabetes. *Pharmacol Res* 37: 233–240, 1998.
26. **Rosen P, Ballhausen T, Bloch W, and Addicks K.** Endothelial relaxation is disturbed by oxidative stress in the diabetic rat heart: influence of tocopherol as antioxidant. *Diabetologia* 38: 1157–1168, 1995.
27. **Shiomi T, Tsutsui H, Ikeuchi M, Matsusaka H, Hayashidani S, Suematsu N, Wen J, Kubota T, and Takeshita A.** Streptozotocin-induced hyperglycemia exacerbates left ventricular remodeling and failure after experimental myocardial infarction. *J Am Coll Cardiol* 42: 165–172, 2003.
28. **Shiomi T, Tsutsui H, Matsusaka H, Murakami K, Hayashidani S, Ikeuchi M, Wen J, Kubota T, Utsumi H, and Takeshita A.** Overexpression of glutathione peroxidase prevents left ventricular remodeling and failure after myocardial infarction in mice. *Circulation* 109: 544–549, 2004.
29. **Siwik DA, Pagano PJ, and Colucci WS.** Oxidative stress regulates collagen synthesis and matrix metalloproteinase activity in cardiac fibroblasts. *Am J Physiol Cell Physiol* 280: C53–C60, 2001.
30. **Siwik DA, Tzortzis JD, Pimental DR, Chang DL, Pagano PJ, Singh K, Sawyer DB, and Colucci WS.** Inhibition of copper-zinc superoxide dismutase induces cell growth, hypertrophic phenotype, and apoptosis in neonatal rat cardiac myocytes in vitro. *Circ Res* 85: 147–153, 1999.
31. **Toussaint O, Houbion A, and Remacle J.** Relationship between the critical level of oxidative stresses and the glutathione peroxidase activity. *Toxicology* 81: 89–101, 1993.
32. **Twigg SM, Cao Z, McLennan SV, Burns WC, Brammar G, Forbes JM, and Cooper ME.** Renal connective tissue growth factor induction in experimental diabetes is prevented by aminoguanidine. *Endocrinology* 143: 4907–4915, 2002.
33. **Vasan RS, Benjamin EJ, and Levy D.** Prevalence, clinical features and prognosis of diastolic heart failure: an epidemiologic perspective. *J Am Coll Cardiol* 26: 1565–1574, 1995.
34. **Welt K, Fitzl G, and Schepper A.** Experimental hypoxia of STZ-diabetic rat myocardium and protective effects of Ginkgo biloba extract. II. Ultrastructural investigation of microvascular endothelium. *Exp Toxicol Pathol* 52: 503–512, 2001.
35. **Yamamoto K, Masuyama T, Sakata Y, Nishikawa N, Mano T, Yoshida J, Miwa T, Sugawara M, Yamaguchi Y, Ookawara T, Suzuki K, and Hori M.** Myocardial stiffness is determined by ventricular fibrosis, but not by compensatory or excessive hypertrophy in hypertensive heart. *Cardiovasc Res* 55: 76–82, 2002.
36. **Ye G, Metreveli NS, Ren J, and Epstein PN.** Metallothionein prevents diabetes-induced deficits in cardiomyocytes by inhibiting reactive oxygen species production. *Diabetes* 52: 777–783, 2003.
37. **Young ME, McNulty P, and Taegtmeyer H.** Adaptation and maladaptation of the heart in diabetes: Part II: potential mechanisms. *Circulation* 105: 1861–1870, 2002.

Thyroid Hormone Inhibits Vascular Remodeling Through Suppression of cAMP Response Element Binding Protein Activity

Kae Fukuyama, Toshihiro Ichiki, Ikuyo Imayama, Hideki Ohtsubo, Hiroki Ono, Yasuko Hashiguchi, Akira Takeshita, Kenji Sunagawa

Objective—Although accumulating evidences suggest that impaired thyroid function is a risk for ischemic heart disease, the molecular mechanism of anti-atherosclerotic effects of thyroid hormone is poorly defined. We examined whether thyroid hormone affects signaling pathway of angiotensin II (Ang II), which is critically involved in a broad aspect of cardiovascular disease process.

Methods and Results—3,3′,5-triiodo-L-thyronine (T3) did not show a significant effect on Ang II-induced activation of extracellular signal-regulated protein kinase or p38 mitogen-activated protein kinase in vascular smooth muscle cells (VSMCs), whereas T3 inhibited Ang II-induced activation of cAMP response element (CRE) binding protein (CREB), a nuclear transcription factor involved in the vascular remodeling process. Coimmunoprecipitaion assay revealed the protein-protein interaction between thyroid hormone receptor and CREB. T3 reduced an expression level of interleukin (IL)-6 mRNA, CRE-dependent promoter activity, and protein synthesis induced by Ang II. Administration of T3 (100 μg/100 g for 14 days) to rats attenuated neointimal formation after balloon injury of carotid artery with reduced CREB activation and BrdU incorporation.

Conclusion—These results suggested that T3 inhibits CREB/CRE signaling pathway and suppresses cytokine expression and VSMCs proliferation, which may account for, at least in part, an anti-atherosclerotic effect of thyroid hormone. (*Arterioscler Thromb Vasc Biol.* **2006;26:2049-2055.**)

Key Words: angiotensin II ■ cAMP response element binding protein ■ thyroid hormone ■ vascular remodeling

Thyroid hormone has various effects on the cardiovascular system. Hypothyroidism is known to be associated with accelerated atherosclerosis and coronary artery disease.[1,2] The Rotterdam study showed that subclinical hypothyroidism is a risk factor for atherosclerosis and myocardial infarction independently of total cholesterol level.[3] It was shown that more angiographic progression of coronary atherosclerosis was documented in patients with the lower serum thyroid hormone level after 2 years of observation.[2,4] These results suggest that thyroid hormone is protective against atherosclerosis; however, the molecular mechanism of anti-atherosclerotic effects has remained to be elucidated.

3,3′,5-triiodo-L-thyronine (T3) is an active form of thyroid hormone, which binds to thyroid hormone receptor (TR). The activated TR recruits transcriptional co-activators and induces gene expression through binding to thyroid hormone response element (TRE) in the promoter region of thyroid hormone responsive genes.[5]

Angiotensin II (Ang II) has multiple biological functions and is involved in a broad aspect of cardiovascular disease process. There are 2 isoforms for Ang II receptor designated type 1 receptor (AT_1R) and type 2 receptor (AT_2R). AT_1R mediates most of the traditional biological effects of Ang II, including vasoconstriction, water and sodium retention, and hypertrophy and hyperplasia of vascular smooth muscle cells (VSMCs). We previously reported that Ang II induced IL-6 expression and vascular hypertrophy through cAMP response element-binding protein (CREB).[6,7] CREB is a 43-kDa nuclear transcription factor bound to cAMP response element (CRE).[8,9] The functional state of CREB is regulated by phosphorylation of serine residue at 133 (Ser133), which promotes association with transcriptional co-activator proteins, CREB-binding protein (CBP) and p300. Overexpression of dominant negative CREB, of which serine 133 is replaced with alanine, attenuated neointimal formation after balloon injury of rat carotid artery.[10]

A recent study showed a physical interaction between TR and CREB[11] in fibroblasts. However, it is not clear whether this novel signaling cross talk affects the vascular remodeling process. We examined the effect of T3 on Ang II signaling pathway and the vascular remodeling process.

Original received December 30, 2005; final version accepted June 5, 2006.

From the Department of Cardiovascular Medicine, Kyushu University Graduate School of Medical Sciences, Fukuoka, Japan.

Consulting Editor for this article was Alan M. Fogelman, MD, Professor of Medicine and Executive Chair, Department of Medicine and Cardiology, UCLA School of Medicine, Los Angeles, Calif.

Correspondence to Toshihiro Ichiki, Department of Cardiovascular Medicine, Kyushu University Graduate School of Medical Sciences, 3-1-1 Maidashi, Higashi-ku, 812-8582 Fukuoka, Japan. E-mail ichiki@cardiol.med.kyushu-u.ac.jp

Arterioscler Thromb Vasc Biol. **is available at http://www.atvbaha.org** **DOI: 10.1161/01.ATV.0000233358.87583.01**

Materials and Methods

Materials

Dulbecco's modified Eagle's medium (DMEM) and fetal bovine serum was purchased from GIBCO BRL. Bovine serum albumin, T3 and an anti-α tubulin antibody were purchased from Sigma-Aldrich, Inc. Ang II was purchased from Peninsula Laboratories, Inc. [^{3}H]-leucine and [^{32}P]α-dCTP were purchased from PerkinElmer Life Sciences. Horseradish peroxidase-conjugated secondary antibodies (anti-rabbit and anti-mouse IgG) were purchased from VECTOR Laboratories Inc. An anti thyroid hormone receptor (anti-TR) antibody that recognizes both TRα and TRβwere purchased from Santa Cruz Biotechnology, Inc. Other antibodies used in the experiments were obtained from Cell Signaling Technology. Other chemical reagents were purchased from Wako Pure chemicals unless specifically mentioned.

Cell Culture

VSMCs were isolated from the thoracic aorta of Sprague-Dawley rats (Kyudo Co; Kamamoto, Japan). Passages between 5 and 13 were used for the experiments as described previously.[6]

Animals

All procedures and care were approved by the Committee on Ethics of Animal Experiments, Kyushu University, and were conducted according to animal care guidelines of the American Physiological Society. Adult male, 12 to 13-week-old Sprague-Dawley rats (350 to 400 g) were anesthetized by intraperitoneal injection of pentobarbital sodium. The left common carotid artery was denuded of the endothelium with a 2-Fr Fogarty balloon catheter (Baxter) that was introduced through the external carotid artery. Inflation and retraction of the balloon catheter were repeated 3 times. Then rats received intraperitoneal injection of T3 (100 μg/100 g body weight suspended in 0.02 N NaOH) every other day for 2 weeks (Hyperthyroid group). Control group received injection of 0.02 N NaOH. Systolic blood pressure and heart rate were measured using tail-cuff method (UR-5000, UEDA). After 2 weeks, rats were euthanized under pentobarbital anesthesia. Carotid arteries were quickly removed and blood samples were collected. Serum concentrations of T3, T4 and thyroid-stimulating hormone (TSH) were measured by radioimmunoassay.

Common carotid artery was ligated just proximal of the bifurcation. The extent of neointimal formation in the just proximal portion of the ligation was examined histologically.

Morphometry and Immunohistochemistry

Serial cross-sections of the carotid rings were stained with hematoxylin and eosin and subjected to morphometry for assessing the intima-media area ratio (I/M ratio) and to immunohistochemistry with the use of the denoted primary antibody and a commercially available detection system as described previously.[10]

Detection of Apoptosis and DNA Synthesis In Vivo

Apoptotic cells were detected by the terminal deoxynucleotidyl transferase (TdT)-mediated dUTP nick end-labeling (TUNEL) method with an apoptosis in situ detection kit (Wako Pure Chemicals) as described previously.[10] In vivo labeling with BrdU (0.5 mg/kg), a thymidine analogue that was injected intraperitoneally 3 hours before preparation of the artery, was performed to identify replicating cells by detection of DNA synthesis. The incorporated BrdU was detected immunohistochemically with an anti-BrdU antibody (Cell proliferation kit, Amersham Pharmacia Biotech) as described previously.[10]

Western Blot Analysis

VSMCs were lysed and Western blot analyses of CREB, extracellular signal-regulated protein kinase (extracellular signal regulated kinase [ERK]) and p38 mitogen-activated protein kinase (p38-MAPK) were performed as described previously.[7]

Immunoprecipitations

VSMCs were lysed in NP-40 lysis buffer[12] and immunoprecipitated with a primary antibody (specific for TR or CREB). Immunoprecipitated proteins were electrophoresed on 12% SDS-PAGE as described previously.[12] An antibody against CREB or TR was used for immunoblotting.

Northern Blot Analysis

Total RNA was prepared according to an acid guanidinium-thiocyanate-phenol-chloroform extraction method. Northern blot analysis for IL-6 and 18S rRNA were performed as described previously.[13]

Measurement of CRE-Dependent Promoter Activity

VSMCs (5×10^5) were prepared in a 6-cm tissue culture dish; 5 μg of CRE (3 copies) /luciferase fusion DNA construct with thymidine kinase (TK) promoter and 2 μg of LacZ gene (driven by simian virus 40 promoter-enhancer sequence) were introduced to VSMCs with the DEAE-dextran method according to the manufacturer's instruction (Promega Corporation). VSMCs were cultured in DMEM with 10% fetal bovine serum for 24 hours, and then incubated with T3 for 30 minutes and stimulated with Ang II (1μmol/L) for 24 hours in DMEM containing 0.1% bovine serum albumin. The luciferase activity was measured and normalized by β-galactosidase activity as described previously.[13]

Measurement of Protein Synthesis

VSMCs were preincubated with T3 for 30 minutes and stimulated with Ang II for 1 hour. Then the medium was changed to a fresh DMEM with 0.1% bovine serum albumin and incubated for additional 23 hours. The cells were labeled with [^{3}H]-leucine during the last 12 hours. Incorporation of [^{3}H]-leucine was measured by a liquid scintillation counter as described previously.[14]

Statistical Analysis

Statistical analysis was performed with 1-way ANOVA and Fisher test if appropriate. Data are shown as mean±SEM. $P<0.05$ was considered to be statistically significant.

Results

T3 Suppressed Ang II-Induced Phosphorylation of CREB at Ser133

We previously reported that Ang II induced CREB activation with a peak at 5 minutes.[7] VSMCs were preincubated with T3 for 30 minutes and stimulated with Ang II for 5 minutes. Western blot analysis using an antibody against phosphorylated form of CREB at Ser133 (P-CREB) was performed. T3 suppressed Ang II-induced phosphorylation of CREB in a dose-dependent manner (Figure 1A). Expression level of total CREB (lower panel) was not affected either by Ang II or T3.

T3 Suppressed CRE-Dependent Transcription Induced by Ang II

A luciferase reporter construct driven by 3 copies of CRE and TK promoter (Figure 1B, left) was introduced VSMCs and luciferase activity was examined. Ang II increased CRE-dependent promoter activity after 24 hours of stimulation, and T3 suppressed the effect of Ang II (Figure 1B).

T3 Had Minimal Effect on Ang II-Induced MAPKs Activation

Ang II induced CREB activation is dependent on ERK and p38MAPK.[7] T3 slightly inhibited the Ang II-induced ERK or

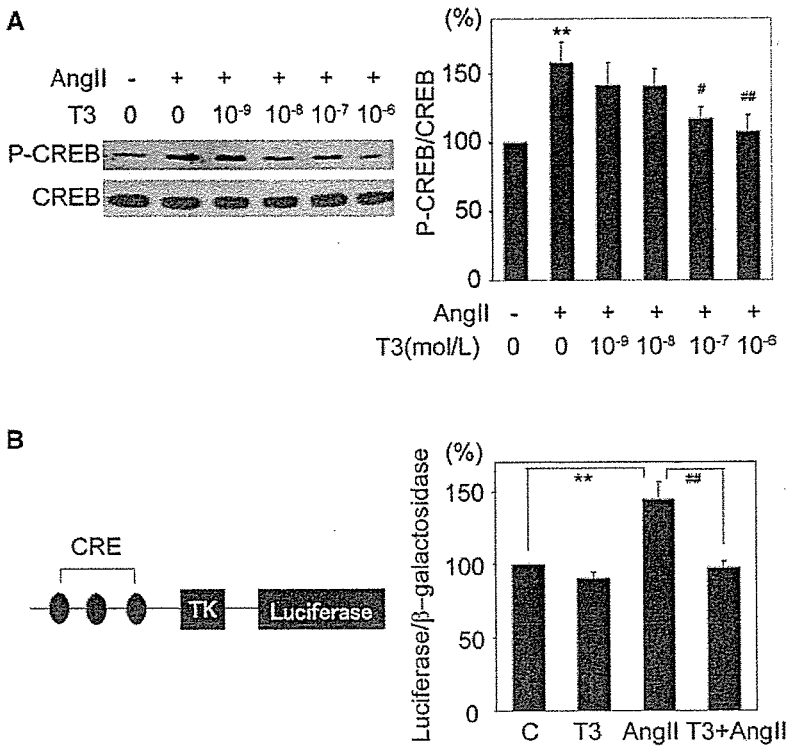

Figure 1. T3 suppressed Ang II-induced phosphorylation of CREB at Ser133. A, VSMCs were preincubated with T3 for 30 minutes at concentrations varying from 10^{-9} to 10^{-6} mol/L and stimulated with Ang II (10^{-7} mol/L) for 5 minutes (n=10). Phosphorylation of CREB was detected by Western blot analysis using a phospho-specific CREB antibody. Density of the specific band was scanned and quantified with an imaging analyzer. The ratio of phosphorylated CREB to total CREB is shown in the right panel. The values (mean±SEM) are expressed as a percent of control (100%). $^{**}P<0.01$ vs control, $^{\#\#}P<0.01$ vs Ang II-stimulated cell, $\#P<0.5$ vs Ang II-stimulated cell. B, CRE (3 copies) /luciferase fusion DNA construct with thymidine kinase promoter (TK) is shown in left panel. The construct and LacZ gene were introduced to VSMCs with the DEAE-dextran method. VSMCs were preincubated with T3 (10^{-6} mol/L) for 30 minutes and stimulated with Ang II (10^{-6} mol/L) for 24 hours (n=4). The luciferase activity was normalized by the β-galactosidase activity. Relative luciferase activity of unstimulated VSMCs (control) was set as 100%. Mean±SEM, $^{**}P<0.01$, $^{*}P<0.05$, $\#\#P<0.01$ vs Ang II-stimulated cell.

p38MAPK phosphorylation as shown in figure 2A and 2B. However, densitometric analysis revealed that inhibition of MAPK phosphorylation by T3 is statistically insignificant (Ang II versus T3+Ang II, pERK; $P=0.182$, p38MAPK; $P=0.135$). Therefore, it was suggested that MAPK does not play a pivotal role in the T3-induced inhibition of CREB phosphorylation.

CREB Interacts With Thyroid Hormone Receptor

Recently, it has been suggested that T3 induced a direct protein–protein interaction between TR and CREB.[11] Immunoprecipitation analysis revealed that CREB was coimmunoprecipitated with TR and vice versa (Figure 2C). However, the amount of associated protein was almost the same between T3-stimulated cells (T3) and nonstimulated cells (C), suggesting that CREB and TR are constitutively interacting.

T3 Suppressed Angiotensin II-Induced IL-6 Expression

It was examined whether T3-induced inhibition of CREB results in the suppression of Ang II-induced gene expression. Preincubation with T3 for 30 minutes reduced the expression level of Ang II-induced IL-6 mRNA, which is dependent on CRE and CREB[6] (Figure 3A).

T3 Inhibited Angiotensin II-Induced Protein Synthesis in VSMCs

The effect of T3 on Ang II-induced incorporation of [^{3}H]-leucine was examined. We previously reported that prolonged expose (>3 hours) to T3 reduced AT_1R expression level in VSMCs.[15] To exclude the possible effect of T3 inhibition of AT_1R expression on Ang II-induced leucine incorporation, the medium was changed to a fresh serum free medium after VSMCs were preincubated with T3 for 30 minutes and stimulated with Ang II for additional 1 hour. Ang II weakly but significantly increased protein synthesis with 1 hour of stimulation and T3 inhibited Ang II-induced protein synthesis (Figure 3B).

Neointimal Formation of Balloon-Injured Artery Was Suppressed in Hyperthyroid Rats

We previously showed that inhibition of CREB function attenuated neointimal formation after vascular injury.[10] We assumed that T3 might show the same effect if T3 inhibits CREB function in vivo. We treated rats with T3 after balloon injury (Table). After 14 days of balloon injury of rat carotid artery, the cross-section of carotid artery showed a substantial neointimal formation (Figure 4A, left). Administration of T3 significantly suppressed the neointimal formation (Figure 4A,

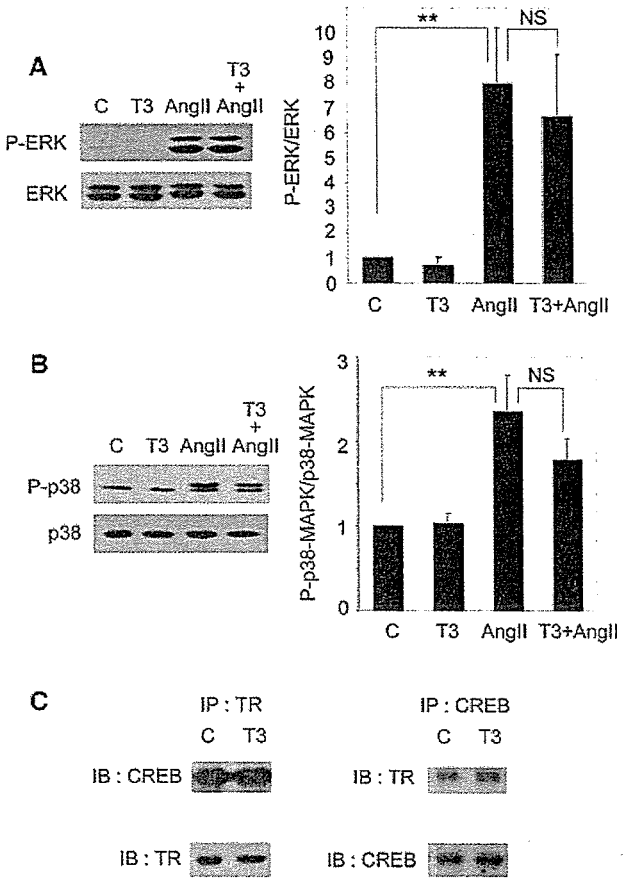

Figure 2. An effect of T3 on Ang II-induced MAP kinase activation. VSMCs were preincubated with T3 (10^{-6} mol/L) for 30 minutes and stimulated with Ang II (10^{-7} mol/L) for 5 minutes. Western blot analysis of (A) phosphorylated ERK (P-ERK) and ERK (n=6), (B) phosphorylated p38-MAPK (P-p38), and p38-MAPK (n=7) were performed as described in the legend to Figure 1. Density of the specific band was scanned and quantified with an imaging analyzer. The ratio of phosphorylated ERK to total ERK and phosphorylated p38-MAPK to total p38-MAPK are shown. $^{**}P<0.05$, NS=not significant. C, VSMCs were stimulated with T3 (10^{-6} mol/L) for 30 minutes, lysed and immunoprecipitated (IP) with an antibody specific to TR (left panel) or an antibody specific to CREB (right panel). Both TR and CREB were detected by immunoblot analysis (IB) as described in the legend to Figure 1. A representative autoradiograph is shown. (n=6)

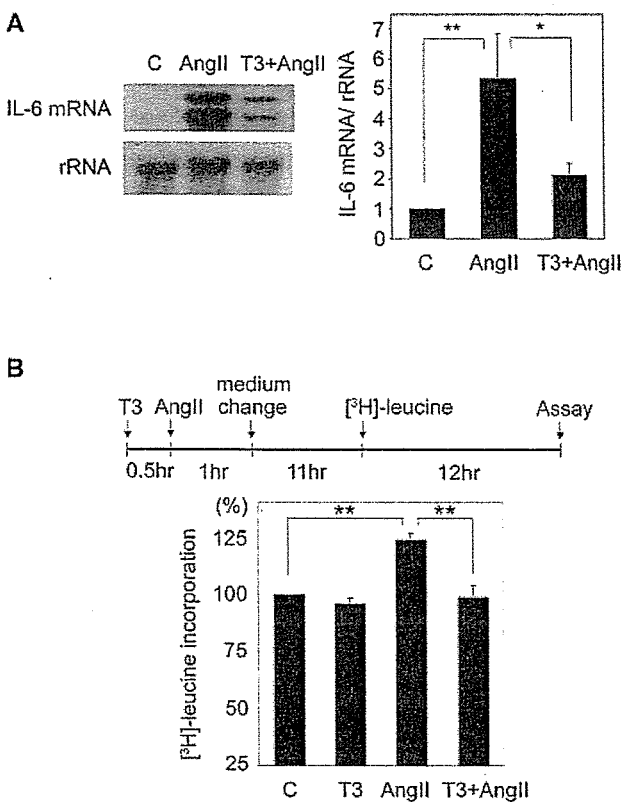

Figure 3. Effects of T3 on Ang II-induced IL-6 mRNA expression and protein synthesis. A, VSMCs were preincubated with T3 (10^{-6} mol/L) for 30 minutes and stimulated with Ang II (10^{-6} mol/L) for another 30 minutes. IL-6 mRNA expression was detected by Northern blot analysis. The radioactivity of the band of IL-6 mRNA was counted by a Bioimage Analyzer and was normalized by that of rRNA. The ratio of radioactivity of IL-6 mRNA to that of rRNA is shown (n=6). The values are expressed as mean±SEM. $^{**}P<0.01$, $^{*}P<0.05$. B, VSMCs were preincubated with T3 (10^{-6} mol/L) for 30 minutes and stimulated with Ang II (10^{-7} mol/L) for 1 hour. The medium was changed to fresh serum free medium and incubated for additional 23 hours. The protocol is shown in the upper panel. Incorporation of $[^3H]$-leucine was measured by a liquid scintillation counter. Results are expressed as mean±SEM. $[^3H]$-leucine incorporation of unstimulated cells was set as 100%. n=9, $^{**}P<0.01$.

right and, 4B). CREB-positive and phosphorylated CREB-positive cells were detected in the neointima of the carotid arteries (Figure 4C). T3 reduced the ratio of phosphorylated CREB positive cells to total cells (Figure 4C upper right panel), whereas the ratio of CREB positive cells to total cells was not changed (Figure 4C lower right panel).

To examine whether T3 induces apoptosis in neointima of balloon-injured artery or not, we detected apoptotic cells with TUNEL method. Although TUNEL index (the ratio of TUNEL positive cells to total cells) were slightly increased in T3-treated rats compared with control, the increase was not statistically significant (Figure 5A). BrdU positive cells were increased in the neointima after 7 days of vascular injury. In T3-treated rats, BrdU labeling index was lower than control group (5.27±1.46% versus 9.73±1.89% in control, $P<0.05$), which suggests that T3 decreased cell proliferation in the neointima of balloon-injured artery (Figure 5B). To exclude the possible effect of high blood flow on the neointimal formation in hyperthyroid state, we examined the extent of neointimal formation in a carotid artery ligation model. The I/M ratio of hyperthyroid rats was also decreased compared with that of control rats in this model (Figure I, available online at http://atvb.ahajournals.org), suggesting that thyroid hormone inhibits neointimal formation, at least in part, through a direct effect on the blood vessel.

Discussion

Ang II plays an important role in atherosclerotic cardiovascular disease and is known to accelerate atherogenesis through vascular hypertrophy, cytokine production, and cell growth.[16–18] Many reports have shown that MAPKs are critically involved in these processes.[7,19] We previously